

1 Projected sea level rise and changes in extreme storm surge and wave 2 events during the 21st century in the region of Singapore

3
4 Heather Cannaby¹, Matthew D. Palmer², Tom Howard², Lucy Bricheno¹, Daley Calvert², Justin
5 Krijnen², Richard Wood², Jonathan Tinker², Chris Bunney², James Harle¹, Andrew Saulter², Clare
6 O'Neill², Clare Bellingham¹, Jason Lowe²

7 ¹National Oceanography Centre, 6 Brownlow Street, Liverpool, L3 5DA, UK

8 ²Met Office, Fitz Roy Road, Exeter, Devon, EX1 3PB, UK

9 Corresponding author contact details: e-mail: heanna@noc.ac.uk, Tel: +44 151 795 4848, Fax: +44
10 (0)151 7954801

11 12 **Abstract**

13 Singapore is an island state with considerable population, industries, commerce and transport located
14 in coastal areas at elevations less than 2 m making it vulnerable to sea-level rise. Mitigation against
15 future inundation events requires a quantitative assessment of risk. To address this need, regional
16 projections of changes in (i) long-term mean sea level and (ii) the frequency of extreme storm surge
17 and wave events have been combined to explore potential changes to coastal flood risk over the 21st
18 century. Local changes in time mean sea level were evaluated using the process-based climate
19 model data and methods presented in the IPCC AR5. Regional surge and wave solutions extending
20 from 1980 to 2100 were generated using ~12 km resolution surge (Nucleus for European Modelling of
21 the Ocean - NEMO) and wave (WaveWatchIII) models. Ocean simulations were forced by output
22 from a selection of four downscaled (~12 km resolution) atmospheric models, forced at the lateral
23 boundaries by global climate model simulations generated for the IPCC AR5. Long-term trends in
24 skew surge and significant wave height were then assessed using a generalised extreme value
25 model, fit to the largest modelled events each year. An additional atmospheric solution downscaled
26 from the ERA-Interim global reanalysis was used to force historical ocean model simulations
27 extending from 1980-2010, enabling a quantitative assessment of model skill. Simulated historical
28 sea surface height and significant wave height time series were compared to tide gauge data and
29 satellite altimetry data respectively. Central estimates of the long-term mean sea level rise at
30 Singapore by 2100 were projected to be 0.52 m(0.74 m) under the RCP 4.5(8.5) scenarios
31 respectively. Trends in surge and significant wave height 2-year return levels were found to be
32 statistically insignificant and/or physically very small under the more severe RCP8.5 scenario. We
33 conclude that changes to long-term mean sea level constitute the dominant signal of change to the
34 projected inundation risk for Singapore during the 21st century. We note that the largest recorded
35 surge residual in the Singapore Strait of ~84 cm lies between the central and upper estimates of sea
36 level rise by 2100, highlighting the vulnerability of the region.

37
38 **Keywords:** Singapore, SE Asia, Sea level rise, Climate change, Significant wave height, Storm surge

41 1. Introduction

42 Singapore is an island state with considerable population, industries, commerce and transport located
43 in coastal areas at elevations less than 2 m (Wong, 1992). Singapore is thus potentially exposed to
44 the effects of sea level rise and climate induced changes in extreme events. Mitigation against future
45 inundation events requires a quantitative assessment of risk. Global scale climate projections
46 generated for the Intergovernmental Panel on Climate Change Assessment Reports (Meehl et al.,
47 2007; Church et al., 2013) are generally on too coarse a grid scale to provide relevant information at
48 the regional scale (e.g. Allen et al., 2010; Penduff et al., 2010). Hence the assessment of climate
49 change impacts on regional coastlines requires a focused regional study. To address this need
50 regional projections of changes in (i) long-term mean sea level and (ii) the frequency of extreme storm
51 surge and wave events have been combined to explore potential changes to coastal flood risk in
52 Singapore over the 21st century. The following paragraphs briefly summarise the processes which
53 influence temporal variability in sea level in the Singapore Strait.

54
55 Located in the middle of the Sunda shelf, the Singapore Strait (Figure 1a) is connected via the South
56 China Sea to the Pacific Ocean in the northeast, to the Java Sea in the southeast, and via the
57 Malacca Strait to the Indian Ocean in the west. Regional tides are complex with several amphidromic
58 points located in the South China Sea. Tides propagate into the Singapore Strait via the Malacca
59 Strait and from the open seas to the east, resulting in a complex mix of diurnal and semi-diurnal tides
60 observed around the coastline of Singapore (Maren and Gerritsen, 2012). The mean tidal range at
61 Singapore is ~2 m and the spring maximum range is ~3 m.

62
63 The weather in Singapore is influenced by the northern and southern hemisphere monsoon systems.
64 Winds are from the north and northeast during the northeast monsoon season, which extends from
65 December to early March and from the south or southeast during the southwest monsoon season
66 which extends from June to September. In response to the monsoon winds, sea level in the
67 Singapore Strait exhibits seasonal variability of the order ± 20 cm, being highest during the northeast
68 monsoon when the fetch is greatest. Extreme sea level anomaly events in Singapore tend to coincide
69 with prolonged (lasting for several days in duration) northeast winds over the South China Sea during
70 this season (e.g. Tkalich et al., 2009). Interannual variability in sea level is dominated by El Nino and
71 La Nina events which cause the Sea Surface Height (SSH) to vary by ± 5 cm, with lower SSH
72 observed during El Nino events (Tkalich *et al.* 2013).

73 The sheltered location of Singapore results in significant wave heights that are typically less than 1 m.
74 Waves of close to 1 m in height occur along the southwest coast during squall events associated with
75 the southwest monsoon. However, extreme wave events occurring during the northwest monsoon
76 have the potential to be more damaging due to the higher sea level during this season.

77 Tkalich et al. (2013) report that sea level in the Singapore strait has been rising at an average rate of
78 1.2-1.7 mm yr⁻¹ between 1975 and 2009, 1.8-2.3 mm yr⁻¹ between 1984 and 2009 and 1.9-4.5 mm
79 yr⁻¹ between 1996 and 2009. The trend is larger than the global mean during the earlier period and
80 smaller during the latter period. Over multi-decadal timescales, accounting for glacial isostatic
81 adjustment, sea level in the Singapore Strait has been rising at approximately the same rate as the
82 global mean. Bird et al. (2010) consider the impact of pre-observational (early Holocene) sea level
83 change on human dispersal in coastal regions of Singapore, and provide evidence of the rapid rate at
84 which regional sea levels changed during this period. The authors suggest sea levels rose at a rate of
85 1.8 m 100 yr⁻¹ between 8900 and 8100 calibrated yr B.P., exhibited little change in between 7800 and
86 7400 calibrated yr B.P. and then a rose by 4–5 m by 6500 calibrated yr B.P.

87

89 2. Methods

90 Change in the long-term climate of extreme sea level can arise due to (i) change in regional time-
91 mean relative sea level and (ii) change in the frequency/intensity of extreme events. There is
92 evidence from dynamical modelling studies based in the North Sea (e.g. Howard et al., 2010; Sterl et
93 al., 2009) and the Gulf of Mexico (e.g. Smith et al., 2010) that these two components of change can
94 be modelled separately and then combined linearly to give a total projected extreme sea level
95 change. This is the approach taken in this study, although we note that this finding is not necessarily
96 applicable to all locations (e.g. Mousavi et al., 2011; Smith 2010).

97 In this study climate projections are generated for two Representative Concentration Pathways
98 (RCPs, Meinshausen et al., 2011), these being RCP4.5 and RCP8.5. The IPCC describe RCP4.5 as
99 an intermediate emissions scenario and it was chosen to provide a moderate mitigation policy
100 scenario. RCP4.5 is comparable to the SRES scenario B1, used in the IPCC AR4 and is consistent
101 with a future with relatively ambitious emissions reductions. RCP8.5 is described as a high emissions
102 scenario and is consistent with a future with no policy changes to reduce emissions. RCP8.5 was
103 chosen to provide an upper estimate of expected change (Meinshausen et al., 2011).

104

105 2.1 Calculation of local changes in time-mean sea level

106 Projections of global mean sea level (GMSL) rise have been presented by the IPCC AR5 (Church et
107 al., 2013) for a range of climate change scenarios. These projections include estimates of: (1) global
108 thermal expansion, (2) ice sheet mass changes from surface mass balance, (3) ice sheet mass
109 changes from ice dynamics, (4) glacier mass changes and (5) changes in land water (from ground
110 water extraction and reservoir impoundment). Time series for each component (1)-(5), under different
111 RCPs, over the 21st Century are available from the IPCC AR5 Chapter 13 supplementary data files
112 (<http://www.climatechange2013.org/report/full-report/>). These time series are derived from the direct
113 output of climate models (1), combining climate model projections with empirical relationships and/or
114 glacier models (2 and 4) and bounding scenarios based on the scientific literature (3 and 5). The
115 upper and lower limits of each time series represent the “likely range” of GMSL change, taking the
116 IPCC AR5 assessment that there is a $\geq 66\%$ chance that the observed sea level rise would fall
117 within these bounds for a given RCP. The additional uncertainty implied by this arises from the
118 authors’ expert judgement of methodological or structural uncertainty that is not captured by the
119 CMIP5 ensemble.

120 Local changes in time mean sea level associated with ocean mass changes (2-5 above) over the 21st
121 Century are evaluated using the fingerprint patterns of Slangen et al. (2014), which represent the ratio
122 of a local sea level change to a unit rise in GMSL for each contributing term. Time series of each term
123 obtained from the AR5 supplementary data files (available at
124 <http://www.climatechange2013.org/report/full-report/>) were converted into local values for Singapore
125 by multiplying by a local scaling factor (Table 1) derived from the Slangen et al. (2014) fingerprints,
126 using the closest 1 x 1 degree grid box. Maps showing the ratio of local relative sea level change per
127 unit of GMSL rise due to Greenland and Antarctica surface mass balance terms and changes in
128 glacial ice content and land water use are shown in Figure 2. Rates of glacial isostatic adjustment
129 (GIA) for Singapore were determined using the combined ice and rheological models ICE-5G(VM2)
130 (Peltier, 2004; <http://www.atmosph.physics.utoronto.ca/~peltier/data.php>), provided by Slangen et
131 al. (2014), again taking data from the closest 1 x 1 degree grid box (Figure 2f). Given the long

132 timescales associated with GIA, the rates of change are assumed to be constant and independent of
133 climate change scenario.

134 Local changes in ocean density (steric change) and circulation are also important for projections of
135 regional sea level (e.g. Pardaens et al., 2011). We follow the approach taken in IPCC AR5 (Church et
136 al., 2013; Slangen et al., 2014) and combine changes in local dynamic sea level (which represents
137 local departures from global mean sea level) with changes in global thermal expansion to estimate the
138 combined effects of local density and ocean circulation (the “oceanographic” term). As has been
139 shown by previous studies (Pardaens et al., 2011, Slangen et al., 2014), we find a large model spread
140 in projections of regional oceanographic sea level rise (Figure 3). However, all models show relatively
141 weak gradients in the pattern of change in the vicinity of Singapore. This result appears to be largely
142 independent of the underlying ocean model resolution, which varies across the CMIP5 models from
143 about 2° to 0.3°

144 The sensitivity of results to the choice of grid box was tested by selecting a primary and secondary
145 grid box to represent Singapore. The difference in multi-model median estimates between boxes is
146 about ± 1 mm and ± 2 mm for RCP4.5 and RCP8.5 respectively. This represents less than 1% of the
147 change signal and therefore is considered a negligible uncertainty. In order to provide an estimate of
148 the projected oceanographic sea level rise that is continuous with time, it was assumed that the
149 change signal (and model spread) emerges proportionally to the global thermal expansion time series
150 of the IPCC AR5. This approach is justified since, to a good approximation, all models show a linear
151 relationship between the local oceanographic sea level change near Singapore, and global thermal
152 expansion (this relationship is demonstrated in Figure A1 for all CMIP5 models for RCP4.5 and
153 RCP8.5). This permits us to estimate the sea level change for the Singapore region throughout the
154 21st century for each scenario.

155 IPCC AR5 estimates of the effect of changes in atmospheric loading for the RCP4.5 and RCP8.5
156 scenarios are available as part of the Chapter 13 supplementary data files (Church et al., 2013).
157 However, the projections for the Singapore region are very small compared to the other terms –
158 representing only about 1% of the total estimated sea level change, with relatively little spread among
159 different model projections. Given the substantial combined uncertainties of the leading terms in total
160 sea level change, we do not include the inverse barometer effect in our final projections as we
161 consider this term constitutes a negligible contribution to projected sea level change.

162 The sea level change for Singapore was computed as the difference between the 1986-2005 and
163 2081-2100 periods. The median of the model ensemble change was taken as the central estimate
164 and the 5th and 95th percentiles were calculated based on the multi-model standard deviation,
165 assuming a normal distribution. Time series of each of the terms listed in Table 1 have a central
166 estimate (based on the median for all terms except the oceanographic term, for which the mean is
167 used) and both an upper and lower bound, which are indicative of the 5th and 95th percentiles of the
168 distribution and/or the likely range assessed in the IPCC AR5. The central estimates of the different
169 components are simply added together to arrive at values for total sea level change at Singapore. To
170 combine the associated uncertainties we follow the approach outlined by Church et al (2013), in which
171 total uncertainty (σ_{tot}) expressed as a variance is estimated according to Eq (1),

$$172 \sigma_{tot}^2 = (\sigma_{ocean} + \sigma_{smb_a} + \sigma_{smb_g})^2 + \sigma_{glac}^2 + \sigma_{LW}^2 + \sigma_{dyn_a}^2 + \sigma_{dyn_g}^2 \quad \text{Eq (1)}$$

173 where σ_{ocean} , σ_{smb_a} , σ_{smb_g} , σ_{glac} , σ_{LW} , σ_{dyn_a} , and σ_{dyn_g} represent uncertainties in sea level rise
174 projections due to changes in oceanographic processes, Antarctic surface mass balance, Greenland
175 surface mass balance, glaciers, land water, Antarctic dynamics and Greenland dynamics respectively.
176 It is assumed that the first three terms which have a strong correlation with global air temperature
177 have correlated uncertainties and can therefore be added linearly. This combined uncertainty is then

178 added to the other components' uncertainties in quadrature. The uncertainties in the projected ice
179 sheet surface mass balance changes are reported to be dominated by the magnitude of climate
180 change, rather than their methodological uncertainty (see AR5 Chapter 13 supplementary materials
181 for details), while the uncertainty in the projected glacier change was assumed to be dominated by
182 methodological uncertainty. We do not include an uncertainty contribution for GIA or the inverse
183 barometer effect (which as noted above has a negligible contribution to sea level projections at
184 Singapore) in our method.

185

186 **2.2 Design of model study**

187 The surge and wave projections described in this work were conducted utilising high resolution (12
188 km) regional atmospheric simulations, forced at the open boundaries by a selection of 9 GCM
189 solutions generated for the IPCC AR5 (IPCC AR4, 2007; see McSweeney et al., 2013 and McSweeney
190 et al 2015 for further details on downscaled atmospheric simulations). Figure 1a shows the
191 downscaled atmospheric model domain. Computational expense dictated the need to select only the
192 most suitable GCMs from which to generate downscaled atmospheric solutions. Approaches for
193 selecting climate models for downscaling are discussed in various papers (e.g. Wilby et al., 2009,
194 Whetton et al 2012). Criteria of particular importance in selecting climate models for impact studies
195 include (a) that the climate models under historical conditions accurately represent the processes or
196 features that are of particular relevance to the impact study and (b) that the climate models sample
197 the range of projected change in the features of interest (Whetton et al, 2012). Both these criteria
198 were considered when selecting models for downscaling. In particular, it was essential that the GCMs
199 used should appropriately represent wind speed during both the northern and southern hemisphere
200 monsoon systems. Selection was further constrained by the availability of suitable data on the CMIP5
201 archive. Of nine downscaled atmospheric simulations conducted, four were selected to force the high
202 resolution surge and wave models: HadGEM2-ES, CNRM-CM5, IPSL-CM5A-MR, and GFDL-CM3.
203 These four models sample a range of projected change in wind speed and include the model GFDL-
204 CM3 which out of the nine downscaled atmospheric simulations exhibited the largest area-averaged
205 change in 850 hPa wind speeds during both the SW and NE monsoon seasons. Computational
206 expense also dictated that downscaled ocean simulations could only be conducted for a single RCP.
207 We therefore chose RCP8.5, which is expected to give the largest climate change signal.

208 Surge and wave climate projections were generated extending from 1970-2100. An additional
209 atmospheric solution downscaled from the ERAinterim (Dee et al., 2011) global atmospheric
210 reanalysis was used to force historical surge and wave simulations extending from 1980-2010. These
211 historical simulations were used to compare model results with contemporary observations.

212

213 **2.3 Description of surge model**

214 The model used to generate surge projections was the Nucleus for European Modelling of the Ocean
215 (NEMO) version 3.4 ocean model (www.nemo-ocean.eu, Madec, 2008). NEMO was run with a
216 horizontal resolution of 1/12th degree and 9 sigma levels in the vertical. The domain extended from
217 95° to 117° East and from 10° South to 17° North as indicated in Figure 1a. Initial conditions specified
218 a constant uniform density and this was maintained throughout the simulations by setting surface heat
219 and salt fluxes to zero. Hence, NEMO was effectively run as a barotropic model. Tidal forcing was
220 applied at the open boundary as a time series of sea-surface elevation representing 15 harmonic tidal
221 constituents: Q1, O1, P1, S1, K1, 2N2, MU2, N2, NU2, M2, L2, T2, S2, K2, M4. In order to allow tides
222 to propagate through the narrow and very shallow (<12 m in places) Strait of Malacca, it was

223 necessary to modify the z-envelope (which allows sigma levels to intercept land in regions of steep
224 topography, thus preventing steep gradients in the vertical levels that may introduce pressure gradient
225 errors) such that the minimum number of vertical levels at any location was 7. The model was run
226 with logarithmic bottom friction and a 4 second barotropic time step. Atmospheric forcing was
227 prescribed as hourly mean sea level pressure and 10 m wind fields. For the case of the 4 GCM-
228 forced simulations, atmospheric forcing was prescribed at the same horizontal resolution as the ocean
229 model. ERAinterim (Dee et al, 2011) atmospheric forcing was prescribed at ~80 km resolution. Sea
230 surface height was recorded at hourly intervals.

231 The climate models used to generate the atmospheric forcing use different calendar years (only
232 CNRM-CM5 uses a Gregorian calendar, GFDL-CM3 and IPSL-CM5A-MR use a 365 day calendar,
233 and HadGEM2-ES uses a 360-day calendar. This introduced difficulties in maintaining consistency
234 between tidal and atmospheric forcing. Consequently the surge model was not run as a transient
235 simulation, rather each year was run independently, following a 5 day spin-up. To avoid splitting
236 model simulations during the winter monsoon period when extreme events are most common, the
237 model was run 360 days forward in time from 1st July. Atmospheric forcing for the 5 day spin-up was
238 taken from the last 5 days of June during the start year of the simulation.

239 The surge metric with which we are concerned in this study is skew surge. Skew surge is the
240 difference between the elevation of the predicted astronomical high tide and the maximum high water
241 observed during the same tidal cycle (e.g. de Vries et al. 1995). Skew surge is considered a more
242 significant and practical measure than surge residual (the difference between the predicted
243 astronomical tide and the observed water level at any time during a tidal cycle). This is because
244 winds are most effective at generating surge in shallow water, meaning peaks in surge residual are
245 typically obtained prior to the predicted high water (Horsburgh and Wilson, 2007). In order to allow
246 calculation of skew surge, an additional NEMO simulation was conducted extending from 1970 to
247 2100 with tidal forcing only (i.e. without any meteorological forcing).

248

249 **2.4 Description of wave model**

250 Wave simulations were performed using WAVEWATCH III (Tolman 1997, 1999a, 2009), a third
251 generation wave model developed by NOAA/NCEP. We used version 3.14 with Tolman and Chalikov
252 (1996) physics. In a spectral wave model, the choice of source terms dictates how the model
253 represents energy input through winds, and dissipation through wave breaking and white capping.
254 Regional validation runs were initially performed using two sets of source terms for comparison: WAM
255 cycle 4 (Monbaliu 2000) and Tolman and Chalikov (1996). The latter has problems with shorter fetch,
256 as wind waves grow slowly and dissipate slowly causing a model bias. WAM cycle 4 has a reduced
257 bias overall but also reduced performance in the tropics. Very little difference was found between
258 these two source terms for the domain of interest and consequently Tolman and Chalikov (1996)
259 source terms were chosen due to the quicker integration time. The regional model was run at 1/12th
260 degree resolution on a grid extending from 95° East to 117° East and 9° South to 14° North as
261 indicated in Figure 1a. The model was run with a global time step of 900 seconds, a spectral
262 resolution of 30 frequency bins, and 24 directional bins. The model was forced at the surface by
263 hourly mean 10 m wind speed at 1/12th degree resolution. Significant wave height, mean wave
264 energy period, mean wave direction, mean directional spread and mean wave period were recorded
265 at hourly intervals. We focus here on projected changes in significant wave height.

266 In order to capture swell incoming at the open boundaries of the regional domain, a 50 km resolution
267 global wave model was also run, forced with 3 hourly wind and daily sea ice values taken from the
268 CMIP5 models. The global WW3 domain consisted of a Spherical Multiple Cell grid with a resolution

269 of 0.7031250° x 0.4687500°, which extended from ~80°N to 80°S. Three-hourly wind data were not
270 available for the entire future period for IPSL-CM5A-MR, and so daily data were used between 2046
271 and 2065. The model produced nest files, which were used to force the regional domain at 3 hour
272 intervals.

273

274 **2.5 Model validation**

275 To assess model performance in simulating local tides, harmonic analyses of modelled and observed
276 sea surface heights were performed using T_TIDE (Pawlowicz et al., 2002). Comparisons were
277 made at four tide gauge stations situated close to Singapore: Raffles Light House, Keling, Tanah
278 Merah, and Kukup (see Figure 1b for locations). Simulated SSH time series were extracted from the
279 closest model grid points to the tide gauge locations. Amplitudes and phases of each tidal constituent
280 were then compared using scatter diagrams. During initial test runs the model was tuned by adjusting
281 the bottom friction parameterisation in order to best represent tidal range, and in particular maximum
282 spring high-water events in the immediate vicinity of Singapore.

283 To assess model performance in representing surge events, simulated annual maximum extreme
284 water levels at grid point 'a' (Figure 1b) were compared to an 18 year (1996-2013) tide-gauge record
285 from Raffles Light House. Six non-overlapping samples of eighteen consecutive years were extracted
286 from each of the model simulations. Return levels were compared to Average Recurrence Interval,
287 (ARI) measured in years. For large return periods ARI is very similar to Return Period (RP; defined as
288 the reciprocal of the annual exceedance probability). ARI and RP are related by Eq (2).

$$289 \quad \text{ARI} = \frac{1}{\log \frac{\text{RP}}{\text{RP}-1}} \quad \text{Eq (2)}$$

290 The advantage of using ARI is that a Gumbel distribution fitted to the tide gauge observations appears
291 as a straight line on a plot of return level versus ARI, even for small ARI. A Gumbel distribution was
292 fitted to the tide gauge observations and to each of the samples of model data, to give a distribution of
293 model scale parameters. This distribution, along with the scale parameter of the observations, is
294 used to assess whether the observations lie comfortably within the distribution of the model samples.

295 Modelled significant wave heights were compared to those derived from EnviSat satellite observations
296 (Atlas et al. 2011), utilising the along-track level-2 data collected between 2003 and 2005. Data were
297 obtained via the Globwave data portal (<http://globwave.ifremer.fr/>). All satellite data falling within the
298 model domain during this period were directly compared to the closest model data point in both space
299 and time. A suite of metrics was then generated from the model-data comparisons: mean errors
300 (ME), root mean square errors (RMS), correlation coefficients (PC) and standard deviations (SD).

301

302 **2.6 Analysis of extreme events**

303 Analysis of extreme skew surge and significant wave height return levels was limited by the length of
304 the model simulation. Furthermore there was considerable inter-annual variability in both modelled
305 and observed extreme water levels, making long-term trends difficult to identify against the
306 background natural variability. To address these limitations a statistical model was used, firstly to
307 derive return levels for periods longer than the period of the simulation, secondly to better model the
308 behaviour of the system at any given return period, and thirdly to make a more informed assessment
309 of the century-scale trends. The model used was the Generalised Extreme Value (GEV) distribution
310 (e.g. Coles, 2001; Hosking *et al.*, 1985; Huerta and Bruno, 2007; Kotz and Nadarajah, 2000; Méndez

311 *et al.*, 2007; 2008) applied to annual maximum skew surge and significant wave height values. We
312 tested the impact of using the R largest events (R ranging from 1 to 5) each year, subject to a
313 separation of at least 120 hours in an effort to ensure independence. Results were not strongly
314 sensitive to the value of R, and furthermore for the GFDL and IPSL simulations the parameter
315 estimates did not remain stable as R increased, which is a requirement for making meaningful use of
316 $R > 1$ (Coles, 2001). Thus for consistency $R = 1$ (annual maxima only) was selected for all simulations.
317 Invoking the External Types Theorem (ETT) we assume that the data are well-approximated by a
318 GEV distribution since each data point is representative of the extreme of a large data block. On
319 fitting a generalised extreme value distribution to the data, the three parameters of the GEV
320 distribution (location, scale and shape) can be used to make statements about the probability of the
321 annual maximum exceeding a particular level. The location parameter of the GEV is analogous to the
322 mean of the normal distribution meaning that a change slides the whole distribution up or down. The
323 scale parameter of the GEV is analogous to the standard deviation of the normal distribution, meaning
324 that an increase widens the spread of the distribution, in the case of the GEV moving the long-period
325 return levels further from the short-period return levels. Thus, a change in either parameter can affect
326 the long-period return levels. In this work we considered the century-scale change in location and
327 scale. It is assumed that the shape parameter remains constant for a given simulation. The GEV
328 distribution was fitted to modelled extreme skew surge and wave heights time series over the 1970-
329 2099 period. Allowing the location parameter to change accommodates potential change in all
330 extreme events (for example at both long and short return periods). Allowing the scale parameter to
331 change accommodates the potential for an increase (or decrease) in the spread of extreme events
332 (for example an increase in intensity of the most extreme surges accompanied by a decrease in
333 intensity of the more frequent surges). A comparison of the quality of the stationary and non-
334 stationary fits gives an indication of the significance of any trend. Linear century-scale trends in return
335 level associated with any given return period were diagnosed from the non-stationary GEV fit to the
336 data. In order to produce a four-model mean (μ) trend estimate, the mean of the ensemble central
337 estimates of trend was taken. The (Bessel-corrected) standard deviation of these four (σ) then
338 represents the uncertainty in the projection. We then identify ($\mu - 1.64 \sigma$) as the lower bound and ($\mu +$
339 1.64σ) as the upper bound. Note that the implied symmetry is in the distribution of trends, not the
340 distribution of the extremes themselves, which will in general be asymmetrical. We note that a
341 limitation of the statistical-modelling is an implicit assumption that the behaviour of the extremes in
342 one year is independent of the behaviour of the extremes in neighbouring years. In fact we expect
343 some autocorrelation due to multi-annual cycles in the climate system. This can reduce the effective
344 number of degrees of freedom compared to the number implied by the assumption of independence.
345 In this circumstance there is a risk of diagnosing a trend as statistically significant simply because the
346 assumed number of degrees of freedom is too large. However, we find *a posteriori* that this is not a
347 big issue in this work since we do not diagnose large significant positive trends.

348
349

350 **3. Model validation**

351 **3.1 Surge Model**

352
353 Comparisons of modelled and observed tidal amplitudes and phases at 4 tide gauge stations (Raffles
354 Light House, Kukup, Tanah Merah, and Keling, located as indicated in Figure 1b) are presented in
355 Figure 4a for the 7 largest tidal constituents (M2, N2, K2, K1, O1, M4 and P1). Modelled tidal
356 amplitudes compare well to those observed, particularly for the dominant semi-diurnal constituents
357 (M2, N2 and K2) for which differences between observed and modelled amplitudes averaged 1.1 cm.
358 The smaller diurnal components (K1, O1, M4, P1) are less well captured by the model with a mean
359 difference between observed and modelled amplitudes of 3 cm. Tidal phase is also well captured by

360 the model (Figure 5b). Modelled and observed tidal phases differed by less than 50°, with the
361 exception at two stations of the smallest amplitude (M4) constituent.

362 Model skill in simulating extreme events is demonstrated by comparing simulated annual maximum
363 extreme water levels at grid point 'a' with annual maximum events extracted from an 18 year (1996-
364 2013) tide-gauge record at Raffles Light House. In order to make a like-for-like comparison, six non-
365 overlapping samples of eighteen consecutive years were extracted from each of the model
366 simulations. This treatment of the 130-year-long simulations as essentially stationary is justifiable in
367 view of the very small trends described in section 4.2. Extreme still-water return levels from each time
368 series are plotted as a function of return period in Figure 5a. Simulated return levels are
369 approximately 20 cm larger than those derived from observations for all return periods. Importantly, it
370 is also evident that the scale parameter (the gradient in Figure 5a) of the model data is comparable to
371 that of the observations. This reveals that the model is doing a good job of simulating the inter-annual
372 variability (or 'spread') in extreme water levels. The Gumbel distribution, fitted to the observations, is
373 shown by the straight line in Figure 6a. The distribution of model scale parameters derived from the
374 Gumbel distribution fitted to each of the samples of model data and the observations, is shown in
375 Figure 5b. (NB. detrending observed and model data had little effect on the results shown in this plot)
376 It can be seen that the scale parameter of the observations lies comfortably within the distribution of
377 the model samples, indicating that the observed scale parameter is well-modelled and that
378 interannual variability in extreme water levels changes little over the course of the simulations. Aside
379 from the mean sea-level uncertainty, it is the uncertainty in the scale parameter that primarily
380 determines the uncertainty in long-period return levels (i.e. the uncertainty in the most extreme
381 events) under the Gumbel distribution. The good agreement between the modelled and observed
382 scale parameter increases our confidence in applying the model to project century-scale changes in
383 extreme water levels.

384 385 **3.2 Wave Model**

386
387 The relationship between simulated significant wave heights and those observed by satellite altimetry
388 across the model domain between 2003 and 2005 is summarised by a correlation coefficient of 0.85,
389 a standard deviation of 0.52 m, and a mean bias of -0.11 m. These statistics demonstrate good
390 model performance, comparable to the UK Met Office's operational wave model performance in
391 tropical regions (Bidlot et al., 2000, Bidlot & Holt, 2006, Bidlot et al., 2007). Qualitative comparison of
392 modelled and observed seasonal mean cycles in significant wave height at Singapore (not shown),
393 demonstrates that the model is able to represent seasonality in significant wave heights at Singapore.
394 A seasonal climatology generated from the ERA-interim forced simulation exhibits maximum
395 significant wave heights of ~0.3 m during the southwest monsoon season and maximum significant
396 wave heights of ~0.35 m during the northeast monsoon season. Significant wave heights decrease to
397 ~0.1 m outside of the monsoon seasons.

398 399 **4. Projections of regional sea level change**

400 **4.1 Time-mean sea level**

401
402 Time series of projected total sea level rise at Singapore and its components for RCP4.5 and RCP8.5
403 are presented in Figure 6. The changes between 1986-2005 and 2081-2100 for each contributing
404 component are presented in Table 2. Central, lower and upper ranges of total sea level rise at
405 Singapore out to 2050 and 2100 are presented in Table 3, alongside global mean values for

406 comparison. The central estimates of total sea level rise at Singapore are similar to the global mean
407 projections reported in the IPCC AR5. Glacier and ice sheet surface mass balance terms result in a
408 larger increase in sea level at Singapore compared to the global mean. This is because there is a far-
409 field rise in sea level as a result of the associated change in Earth's gravity field as the mass is re-
410 distributed away from high latitudes (Tamisiea and Mitrovica, 2011). The larger ice mass balance
411 term is, however, offset by a negative contribution to sea level rise at Singapore from glacial isostatic
412 adjustment. This is the result of additional ocean mass from the last deglaciation depressing the sea
413 floor and causing mantle material to flow underneath the continents causing uplift (Tamisiea et al.,
414 2014).

415 The uncertainty in projections of sea level rise at Singapore is substantially larger than for global
416 mean projections, mainly due to the additional uncertainty associated with representation of regional
417 oceanographic processes (the oceanographic contribution to sea level change) by the coarse
418 resolution CMIP5 models. Scaling up of the ice sheet and glacier terms using the Slangen et al.
419 (2014) fingerprints also contributed to the increased uncertainty of the regional projections. This
420 increased uncertainty is larger for RCP8.5 than for RCP4.5. Over the first half of the 21st Century the
421 projected rate of sea level rise is similar for both RCP4.5 and RCP8.5. Hence on this timescale, sea
422 level rise projections are largely independent of emissions pathway, meaning the uncertainty range is
423 dominated by methodological and model uncertainty. In both RCP4.5 and RCP8.5 there is a
424 substantial acceleration in the rate of sea level rise over the 21st Century, particularly during the early
425 and mid-periods of the 21st century. A simple linear extrapolation of observed long-term regional
426 trends (as reported for Singapore by Tkalich et al., 2013) is therefore likely to grossly underestimate
427 future sea level rise.

428

429 **4.2 Surge changes**

430

431 Time series of annual maximum skew surge at grid point 'a' from each of the four model simulations
432 are presented in Figure 7. (NB. projected changes in surge and significant wave height both have
433 very large spatial scales compared with the scale of Singapore. As a result, it was found that choice
434 of model grid point did not significantly impact the results.) For consistency all skew surge and
435 significant wave height results presented in this paper are taken from grid point 'a' (see Figure 1 for
436 location). For each simulation a non-stationary GEV model fit to the annual maximum significant
437 wave height time series was used to diagnose a linear century-scale trend in return level associated
438 with any given return period. For each simulation the P value associated with the improvement in fit
439 on moving from a stationary to a non-stationary GEV model is quoted in Figure 7. There is always
440 some model improvement with a non-stationary fit because more parameters are added to the
441 statistical model (i.e. a linear time-variation in both location and scale). Taking the CNRM model as
442 an example, the P value is 77%, meaning the small amount of apparent non-stationarity in the CNRM
443 data could easily arise by chance from random variations in stationary data. Thus we cannot discount
444 our null hypothesis of stationarity in the CNRM data. The IPSL model, on the other hand, is consistent
445 with a visual assessment of the data. The P value is very small and we conclude that this data is
446 unlikely to arise from a truly stationary process. Visually, there is a strong suggestion in the IPSL data
447 of a reduction in interannual variability over the 21st century. The standard diagnostic of the quality of
448 the fit of the stationary GEV distribution to the annual mean skew surge data for each simulation is
449 included in Appendix A2 for each of the simulations. Projected century-scale trends in return level are
450 reported in Table 4 and shown diagrammatically in Figure 8. Treating the four models as a small
451 ensemble of equally plausible simulations, we obtain an ensemble [5%ile, 95%ile] of the diagnosed
452 trend in the one hundred-year return level of [-63 , 30] mm/century. We do not find a statistically
453 significant trend in skew surge for any of the return levels tested. Uncertainties in skew surge trends
454 are small compared to the uncertainties in projected mean sea-level change of for example [450,

455 1020] mm (see Table 3) over the 21st century under RCP8.5. As no statistically significant trends in
456 skew surge return levels are projected for RCP8.5, we would not expect to find trends for the less
457 severe RCP4.5 scenario.

458

459

460 **4.3 Wave changes**

461

462 Time series of annual maximum significant wave height at grid point 'a' from each of the four
463 simulations are presented in Figure 9. The standard diagnostic of the quality of the fit of the
464 stationary GEV distribution to the significant wave height and annual maxima for each simulation is
465 shown in Appendix A3. All of the resulting projections of century-scale trends were small and
466 negative, with the exception of the IPSL forced simulation for which a 35 mm century⁻¹ increase in the
467 2-year return level was obtained. The model ensemble of the diagnosed trend in 100-year significant
468 wave height return level is [-0.73 , 0.29] mm century⁻¹. Diagnosed trends in 2, 20, 100, 1000, and
469 10000-year return levels are given in Table 5 and presented diagrammatically in Figure 10. The small
470 sample size of four climate models and the large spread in projections of century-scale change in
471 significant wave height at long return periods means that we cannot rule out positive trends, even
472 though the central estimates of the trends are small and negative in each of the four models.

473

474 **5. Discussion**

475 The overriding conclusion from this study is that change in time mean sea level will be the dominant
476 process influencing the changing vulnerability of Singapore to coastal inundation over the 21st
477 Century. Several studies have drawn similar conclusions for other parts of the world e.g. in the North
478 Sea (Sterl et al., 2009), around the UK (Lowe et al., 2009) and globally (Bindoff et al., 2007). It is
479 notable that the central estimates of sea level rise by 2100 (of 0.52 m and 0.74 m under the RCP4.5
480 and RCP8.5 scenarios respectively) are of similar magnitude to the most damaging surge events
481 recorded at Singapore over recent decades (In describing extreme events occurring since the 1970s,
482 Tkalic et al. (2009) report sea level anomalies ranging from 43 cm to ~60 cm). Hence Singapore is a
483 country particularly vulnerable to sea level rise. Wong (1992) previously highlighted this vulnerability,
484 noting that by adding 1 m to current chart datum levels at Singapore (comparable to our upper
485 estimate of a 1.02 m sea level rise by 2100) the mean spring high water level of 3.8 m will be close to
486 the highest recorded water level to date, of 3.9 m.

487 The climate simulations presented in this work suggest there will be no significant change in the
488 frequency of extreme storm surge or wave events during the 21st century over and above that due to
489 mean sea-level rise. Extreme events of the magnitude seen over recent decades will, however, have
490 a much greater impact when superimposed on rising sea levels. Those involved in mitigating the
491 potential impacts of future climate change on Singapore's coastline therefore need to combine
492 projections of sea level rise with skew surge return level data. Site specific projections of future
493 extreme still water level can be obtained by linearly combining return levels derived from tide gauge
494 data with the sea level change projections presented in Table 3. (Tide-gauge data represent the best
495 information available about present-day location-specific return levels, however, it is worth noting that
496 uncertainties in the present-day return levels derived from relatively short tide-gauge records are likely
497 to be a large component of the combined uncertainty in projected future return-level curves.) In the
498 longer term there is potential to develop better estimates of current risk by combining model-derived
499 information with observed time series. The skew surge joint probability method (Batstone et al., 2013)
500 provides an approach to addressing this problem.

501 There are several caveats to the sea level, surge and wave projections presented in this study and we
502 consider each in turn in the following paragraphs. Mean sea level projections are presented as likely
503 (66–100 % probability) ranges for the RCP4.5 and RCP8.5 climate change scenarios, taking into
504 account a number of uncertainties that cannot be robustly quantified with the present state of scientific
505 knowledge. We note that recent studies have attempted to provide information outside of the IPCC
506 likely range (Kopp et al., 2014 Jevrejeva et al., 2014) and this is an important topic of ongoing
507 discussion by the research community (Hinkel et al., 2015). As noted previously, our sea level
508 projections do not account for the unlikely event of a collapse of the marine-based sectors of the
509 Antarctic ice sheet. Based on current understanding, AR5 assessed that such a collapse, if initiated,
510 could cause global mean sea level to rise substantially above the given likely range during the 21st
511 century. This potential additional contribution cannot be precisely quantified, but the AR5 report
512 assessed with medium confidence that it would not exceed several tenths of a metre of sea level rise
513 during the 21st century (Church et al, 2013). This remains one of the most important structural
514 uncertainties in projecting sea level extremes. An additional source of uncertainty arises from taking
515 patterns of change associated with land ice, land water and GIA from a single source (i.e. the maps
516 generated by Slangen et al., 2014). While Slangen's data are considered very credible estimates
517 based on current understanding, we do not include here any estimate of uncertainties in sea level
518 change that could arise from using alternative estimates of these patterns. The CMIP5 models, due
519 to their low resolution, have limited ability to represent meso-scale hydrographic processes important
520 to regional dynamics. Previous studies (e.g. Lowe et al., 2009 and Perrette et al., 2013), suggest,
521 however, that large-scale oceanic signals propagate freely into the coastal region, and are not overtly
522 affected by the coarse resolution of the models. In common with previous studies (e.g. Lowe et al.,
523 2009 and Perrette et al., 2013), we assume that large-scale oceanic signals propagate freely into the
524 coastal region. The effects of anthropogenic disturbance such as resource extraction and land
525 reclamation on sea level projections are also not considered in this work. Finally, it is important to
526 note that the probability attributed to the sea level projections is calculated without accounting for the
527 potential effects of future seismic activity; the only vertical land movement process considered in this
528 study being glacial-isostatic adjustment. It is possible that vertical land movement associated with
529 seismic activity may dominate changes in relative sea level over decadal time scales. The Earth
530 Observatory of Singapore state that:

531 “Sea level could rise faster than the IPCC predicted after a big earthquake on the Sunda
532 Megathrust. This is due to the overall tectonics of the region. After a big earthquake on the
533 megathrust, the whole Sunda shelf will experience a subsidence.”
534 (<http://www.earthobservatory.sg/faq-on-earth-sciences/singapore-threatened-earthquakes-0>).

535 There are a number of further caveats associated with the modelling of extreme events. Waves and
536 surge have been modelled separately, meaning wave-surge interactions are not accounted for.
537 Surge propagation from outside the boundaries of the surge model domain is also not considered
538 (except by application of a static inverse barometer effect at the boundaries). Over shallow seas,
539 however, wind is the dominant factor in surge generation, suggesting that surge propagation from
540 outside the boundaries will not be a dominant factor in driving extreme water levels on the Sunda
541 shelf (Horsburgh and Wilson, 2007). The impacts of changes in mean water depth on tidal resonance
542 and on surge propagation are also not considered in this work. Pickering (2014) investigated the
543 impact on tidal dynamics of raising GMSL by 2 m and found a change in mean high water level of the
544 order 10 cm around Singapore. Howard et al. (2010), Sterl et al. (2009), and Lowe et al. (2001) find in
545 studies of the northwest European shelf that changing the water depth affects the time of arrival of a
546 storm surge, but not the surge height. Hence, we suggest that any impact of rising sea levels on tidal
547 dynamics will be small compared to sea level rise. Finally, our simulations assume a fixed coastline
548 with no inundation. Further work with a high resolution inundation model is required to understand the

549 land area at risk from inundation due to sea level rise, and to design appropriate coastal defences to
550 best mitigate this risk.

551

552 **6. Conclusions**

553 Regional projections of changes in long-term mean sea level and in the frequency of extreme storm
554 surge and wave events over the 21st century have been generated for Singapore. Local changes in
555 time mean sea level were evaluated using the process-based climate model data and methods
556 presented in the IPCC AR5. Regional surge and wave forecast simulations extending from 1970 to
557 2100 were generated using high resolution (~12 km) regional surge (Nucleus for European Modelling
558 of the Ocean - NEMO) and wave (WaveWatchIII) models. Ocean simulations were forced by four
559 regional atmospheric model solutions, which were in turn nested within global atmospheric
560 simulations generated for the IPCC AR4. The four climate models were chosen to best represent
561 historical conditions and included the GFDL-CM3 model which exhibited the largest area-averaged
562 changes in 850 hPa wind speeds during both the SW and NE monsoon seasons. An additional
563 atmospheric regional model simulation driven by a global atmospheric reanalysis was used to force
564 historical regional ocean model simulations extending from 1980-2010. The hindcast simulation was
565 used to demonstrate the skill of the models in simulating regional tides and surge events (through
566 comparison to tide gauge data) and significant wave heights (through comparison to satellite altimetry
567 data).

568 Central estimates of long-term mean sea level rise at Singapore by 2100 are projected to be
569 0.52 m (0.74 m) under the RCP 4.5(8.5) scenarios respectively. These values are very close to the
570 global mean estimates presented in the IPCC AR5. Sea level rise at Singapore resulting from mass
571 loss from ice sheets and glaciers is projected to be 10-15% larger than the global mean. This will,
572 however, be offset by elevation of the land mass due to glacial isostatic adjustment. The likely ranges
573 of projected sea level rise at Singapore are substantially larger than the global mean projections,
574 mainly due to the uncertainty associated with representation of regional oceanographic processes by
575 the coarse resolution CMIP5 models. Due to an acceleration in the rate of sea level rise throughout
576 the early and mid- 21st century, extrapolation of long-term tide-gauge records does not provide
577 reliable estimates of future sea level change and systematically underestimates the magnitude of
578 future sea level rise for both scenarios.

579 The [5%ile, 95%ile] of diagnosed trend in one hundred-year skew surge return level, obtained by
580 treating the four models as a small ensemble of equally plausible simulations is
581 [-63, 30] mm century⁻¹. The corresponding [5%ile, 95%ile] of the diagnosed trend in one hundred-
582 year significant wave height return level is [-0.73 , 0.29] mm century⁻¹. The uncertainties in projected
583 century-scale trend in skew surge and significant wave height are small compared to the uncertainties
584 in projected mean sea-level change of for example [450, 1020] mm over the 21st century under
585 RCP8.5. We find no statistically significant changes in extreme skew surge events and no statistically
586 significant changes in extreme significant wave height under the RCP 8.5 scenario over and above
587 that due to mean sea-level change using the four model ensembles. Our primary finding is then that
588 change in time mean sea level will be the dominant process influencing the changing vulnerability of
589 Singapore to coastal inundation over the 21st Century. We note that the largest recorded surge
590 residual in the Singapore Strait of ~84 cm (Tkalic et al., 2009) lies between the central and upper
591 estimates of sea level rise by 2100.

592

593 **Acknowledgements**

594 This study was carried out as part of Singapore's Second National Climate Change Study and was
595 funded by the government of Singapore. Full reports of the study can be found of the Centre for
596 Climate Research Singapore (CCRS) website at [http://ccrs.weather.gov.sg/publications-second-](http://ccrs.weather.gov.sg/publications-second-National-Climate-Change-Study-Science-Reports)
597 [National-Climate-Change-Study-Science-Reports](http://ccrs.weather.gov.sg/publications-second-National-Climate-Change-Study-Science-Reports).

598 Jamie Kettleborough and Ian Edmond provided scripts for downloading and archiving the CMIP5 data
599 used in this study. We thank Aimée Slangen for providing spatial fingerprint data used in the
600 projections of regional sea level change and Mark Carson for assistance with carrying out the
601 comparison with the Slangen et al (2014) oceanographic sea level changes. We acknowledge use of
602 the MONSooN system, a collaborative facility supplied under the Joint Weather and Climate
603 Research Programme, which is a strategic partnership between the Met Office and the Natural
604 Environment Research Council. This work also used the ARCHER UK National Supercomputing
605 Service (<http://www.archer.ac.uk>).

606

607 **References**

608 Allen JI, Aiken J, Anderson TR, Buitenhuis E, Cornell S, Geider R, Haines K, Hirata T, Holt J, Le
609 Quéré C, Hardman-Mountford N, Ross ON, Sinha B, While J (2010) Marine ecosystem models for
610 earth systems applications: the MarQUEST experience. *Journal of Marine Systems* 81, 19–33.

611

612 Atlas R, Hoffman RN, Ardizzone J, Leidner SM, Jusem JC, Smith DK, Gombos D (2011) A cross-
613 calibrated, multiplatform ocean surface wind velocity product for meteorological and oceanographic
614 applications. *Bull. Amer. Meteor. Soc.*, 92:157-174. doi: 10.1175/2010BAMS2946.1

615 Batstone C, Lawless M, Tawn J, Horsburgh K, Blackman D, McMillan A, Worth D, Laeger S, Hunt T
616 (2013) A UK best-practice approach for extreme sea-level analysis along complex topographic
617 coastlines. *Ocean Engineering*, 71:28-39. 10.1016/j.oceaneng.2013.02.003

618 Bidlot JR, Holmes-Bell DJ, Wittmann PA, Lalbeharry R, Chen HS (2000) Intercomparison of the
619 performance of operational ocean wave forecasting systems with buoy data. *European Centre for
620 Medium-Range Weather Forecasts (ECMWF) Technical Memorandum Number 315 also 2002,*
621 *Weather and Forecasting*, 17:287-310.

622 Bidlot JR, Li LG, Wittmann P, Fauchon M, Chen H, Lefevre JM, Bruns T, Greenslade D, Arduin F,
623 Kohno N, Park S, Gomez M (2007) Inter-comparison of operational wave forecasting systems. 10th
624 International Workshop on Wave Hindcasting and Forecasting and Coastal Hazard Symposium, North
625 Shore, Oahu, Hawaii, 11-16 November 2007.

626 Bidlot JR, Holt MW (2006) Verification of operational global and regional wave forecasting systems
627 against measurements from moored buoys. *JCOMM Technical Report*, 30. WMO/TDNo.1333.

628 Bindoff NL, Willebrand J, Artale V, Cazenave A, Gregory J, Gulev S, Hanawa K, Le Quéré C, Levitus
629 S, Nojiri Y, Shum CK, Talley LD, Unnikrishnan A (2007) Observations: Oceanic Climate Change and
630 Sea Level. In: *Climate Change 2007: The Physical Science Basis. Contribution of Working Group I to
631 the Fourth Assessment Report of the Intergovernmental Panel on Climate Change [Solomon S, Qin
632 D, Manning M, Chen Z, Marquis M, Averyt KB, Tignor M, Miller HL (eds.)]. Cambridge University
633 Press, Cambridge, United Kingdom and New York, NY, USA.*

634 Bird MI, Austin WEN, Wurster CM, Fifield LK, Mojtahis M, Sargeant C (2010) Punctuated eustatic
635 sea-level rise in the early mid-Holocene. *Geology*, 38(9), 803-806, 2010;38:803–6.
636 doi:10.1130/G31066.1

637 Church JA, et al. (2013) Sea Level Change. In: *Climate Change 2013: The Physical Science Basis.*
638 *Contribution of Working Group I to the Fifth Assessment Report of the Intergovernmental Panel on*
639 *Climate Change* [Stocker TF, Qin D, Plattner GK, Tignor M, Allen SK, Boschung J, Nauels A, Xia Y,
640 Bex V, Midgley PM (eds.)]. Cambridge University Press, Cambridge, United Kingdom and New York,
641 NY, USA.

642 Church JA, et al. (2001) Changes in sea level. In: *Climate Change 2001: The Scientific Basis.*
643 *Contribution of Working Group I to the Third Assessment Report of the Intergovernmental Panel on*
644 *Climate Change* [Houghton JT, et al. (eds.)]. Cambridge University Press, Cambridge, United
645 Kingdom and New York, NY, USA, pp. 639–693.

646 Coles S (2001) An introduction to statistical modeling of extreme values. pp 208. London: Springer,
647 2001.

648 Dee DP, Uppala SM, Simmons AJ, Berrisford P, Poli P, Kobayashi S, Andrae U, Balmaseda M A,
649 Balsamo G, Bauer P, Bechtold P, Beljaars ACM, van de Berg L, Bidlot J, Bormann N, Delsol C,
650 Dragani R, Fuentes M, Geer AJ, Haimberger L, Healy SB, Hersbach H, Hólm EV, Isaksen L, Kållberg
651 P, Köhler M, Matricardi M, McNally AP, Monge-Sanz BM, Morcrette JJ, Park BK, Peubey C, de
652 Rosnay P, Tavolato C, Thépaut JN, Vitart F (2011), The ERA-Interim reanalysis: configuration and
653 performance of the data assimilation system. *Q.J.R. Meteorol. Soc.*, 137: 553–597. doi:
654 10.1002/qj.828

655 de Vries H, Breton M, de Mulder T, Krestenitis Y, Ozer J, Proctor R, Ruddick K, Saloman JC, Voorrips
656 A (1995) A comparison of 2D storm-surge models applied to three shallow European seas.
657 *Environmental Software*, 10(1):23-42.

658 Hinkel J, Jaeger C, Nicholls RJ, Lowe J, Renn O, Peijun S (2015) Sea-level rise scenarios and
659 coastal risk management, *Nature Climate Change*, 5, 188–190. doi:10.1038/nclimate2505.

660 Horsburgh KJ, Wilson, C (2007) Tide-surge interaction and its role in the distribution of surge
661 residuals in the North Sea. *Journal of Geophysical Research*, 112 (C8). Art. No. C08003.
662 10.1029/2006JC004033.

663 Hosking JRM, Wallis JR, Wood EF (1985) Estimation of the generalized extreme-value distribution by
664 the method of probability-weighted moments. *Technometrics* 27(3):251-261.

665 Howard T, Lowe J, Horsburgh K (2010) Interpreting century-scale changes in southern North Sea
666 storm surge climate derived from coupled model simulations. *Journal of Climate* 23(23):6234-6247.

667 Howard T, Pardaens AK, Bamber JL, Ridley J, Spada G, Hurkmans RTWL, Lowe JA, Vaughan D
668 (2014) Sources of 21st century regional sea-level rise along the coast of northwest Europe, *Ocean*
669 *Sci.*, 10:473-483, doi: 10.5194/os-10-473-2014.

670 Huerta G, Bruno S (2007) Time-varying models for extreme values. *Environmental and Ecological*
671 *Statistics* 14(3):285-299.

672 IPCC AR4 (2007) *Climate change 2007. The physical science basis. Summary for policymakers.* In:
673 Alley R, Berntsen T, Bindoff NL, et al. (Eds.), *Contribution of Working Group I to the Fourth*
674 *Assessment Report of the Intergovernmental Panel on Climate Change.*

675 Kotz S, Nadarajah S (2000) *Extreme Value Distributions: Theory and Applications*. London: Imperial
676 College Press, 2000.

677 Kopp RE, Horton RM, Little CM, Mitrovica JX, Oppenheimer M, Rasmussen DJ, Strauss BH, Tebaldi
678 C (2014) Probabilistic 21st and 22nd century sea-level projections at a global network of tide-gauge
679 sites. *Earth's future*. 2(8), 383-406.

680 Lowe JA, Howard TP, Pardaens A, Tinker J, Holt J, Wakelin S, Milne G, Leake J, Wolf J, Horsburgh
681 K, Reeder T, Jenkins G, Ridley J, Dye S, Bradley S (2009) UK Climate Projections science report:
682 Marine and coastal projections. Met Office Hadley Centre, Exeter, UK.

683 Lowe JA, Gregory J, Flather R (2001) Changes in the occurrence of storm surges around the United
684 Kingdom under a future climate scenario using a dynamic storm surge model driven by the Hadley
685 Centre climate models. *Clim. Dynam.*, 18 (3-4):179–188.

686 Madec G (2008) NEMO reference manual 3_4_STABLE : "NEMO ocean engine". Note du Pôle de
687 modélisation, Institut Pierre-Simon Laplace (IPSL), France, No 27 ISSN No 1288-1619.

688 Maren DV, Gerritsen H (2012) Residual flow and tidal asymmetry in the Singapore Strait, with
689 implications for resuspension and residual transport of sediment. *Journal of Geophysical Research*,
690 117, C04021, doi:10.1029/2011JC007615.

691 McSweeney C, Rahmat R, Redmond G, Marzin C, Murphy J, Jones R, Cheong WK, Lim SY, Sun X
692 (2015) Singapore's Second National Climate Change Study – Phase 1: Chapter 3: Sub-selection of
693 CMIP5 GCMs for downscaling over Singapore. [Web link: [http://ccrs.weather.gov.sg/publications-
694 second-National-Climate-Change-Study-Science-Reports](http://ccrs.weather.gov.sg/publications-second-National-Climate-Change-Study-Science-Reports)]

695 McSweeney CF, Jones RG, Lee RW, Rowell DP (2015) Selecting CMIP5 GCMs for downscaling
696 over multiple regions. *Climate Dynamics*, 44:3237-3260.

697 Mendez FJ, Menendez M, Luceo A, Losada IJ (2008) Estimation of the long-term variability of
698 extreme significant wave height using a time-dependent Peak Over Threshold (POT) model, *J.*
699 *Geophys. Res.*, 111:C07024, doi:10.1029/2005JC003344.

700 Méndez FJ, Menéndez M, Luceño A, Losada IJ (2007) Analyzing Monthly Extreme Sea Levels with a
701 Time-Dependent GEV Model. *J. Atmos. Oceanic Technol.*, 24:894–911. doi:
702 <http://dx.doi.org/10.1175/JTECH2009.1>

703 Meinshausen M, Smith SJ, Calvin KV, Daniel JS, Kainuma MLT, Lamarque JF, Matsumoto K, S.
704 Montzka SA, Raper SCB, Riahi K, Thomson AM, Velders GJM van Vuuren D (2011) The RCP
705 Greenhouse Gas Concentrations and their Extension from 1765 to 2300. *Climatic Change (Special
706 Issue)*, DOI: 10.1007/s10584-011-0156-z.

707 Monbaliu J et al. (2000) "The spectral wave model, WAM, adapted for applications with high spatial
708 resolution." *Coastal engineering* 41(1):41-62.

709 Mousavi M, Irish J, Frey A, Olivera F, Edge B (2011) Global warming and hurricanes: The potential
710 impact of hurricane intensification and sea level rise on coastal flooding. *Clim. Change*, 104:575–597.

711 Pardaens A, Gregory, JM Lowe, J (2011) A model study of factors influencing projected changes in
712 regional sea level over the twenty-first century. *Clim. Dyn.*, 36:2015–2033.

713 Pawlowicz R, Beardsley B, Lentz S (2002) Classical Tidal Harmonic Analysis Including Error
714 Estimates in MATLAB using T_TIDE", *Computers and Geosciences*, 28:929-937.

715 Peltier WR (2004) Global Glacial Isostasy and the Surface of the Ice-Age Earth: The ICE-5G (VM2)
716 Model and GRACE, *Ann. Rev. Earth and Planet. Sci.*, 32, 111-149.

717 Penduff T, Juza M, Brodeau L, Smith GC, Barnier B, Molines JM, Treguier AM, Madec G (2010)
718 Impact of global ocean model resolution on sea-level variability with emphasis on interannual time
719 scales. *Ocean Science*, 6, 269–284.
720

721 Perrette, M., Landerer, F., Riva, R., Frieler, K., and Meinshausen, M (2013), A scaling approach to
722 project regional sea level rise and its uncertainties. *Earth System Dynamics*, 4(1), 11–29.
723 doi:10.5194/esd-4-11-2013

724 Pickering M (2014) The impact of future sea-level rise on the tides. University of Southampton, Ocean
725 and Earth Science, Doctoral Thesis , 347pp.

726 Slangen ABA, Carson M, Katsman, CA, van de Wal RSW, Koehl A, Vermeersen, LLA Stammer D
727 (2014) Projecting twenty-first century regional sea-level changes, *Climatic Change*, doi:
728 10.1007/s10584-014-1080-9.

729 Jevrejeva S, Grinsted A, Moore CJ (2014) Upper limit for sea level projections by 2100.
730 *Environmental Research letters*, 9, 1-9.

731 Smith JM, Cialone MA Wamsley TV McAlpin TO (2010) Potential impact of sea level rise on coastal
732 surges in southeast Louisiana. *Ocean Eng.*, 37:37–47.

733 Sterl A, van den Brink H, de Vries H, Haarsma R, van Meijgaard E (2009) An ensemble study of
734 extreme North Sea storm surges in a changing climate. *Ocean Sci.*, 5:369–378.

735 Tamisiea ME, Mitrovica JX (2011) The moving boundaries of sea level change: Understanding the
736 origins of geographic variability. *Oceanography* 24(2):24–39, doi:10.5670/oceanog.2011.25.

737 Tamisiea ME, Hughes CW, Williams SDP, Bingley RM (2014) Sea level: measuring the bounding
738 surfaces of the ocean. *Philosophical Transactions of the Royal Society of London, A*, 372: 2025.
739 20130336. 10.1098/rsta.2013.0336

740 Tkalich, P, Vethamony P, Babu MT, Pokratath R (2009) Seasonal sea level variability and anomalies
741 in the Singapore Strait. *Proceedings of International Conference in Ocean Engineering, ICOE 2009*
742 IIT Madras, Chennai, India. 1-5 Feb. 2009

743 Tkalich P, Vethamony P. Luu QH, Babu MT (2013), Sea level trend and variability in the Singapore
744 Strait, *Ocean Sci.*, 9, 293-300, doi:10.5194/os-9-293-2013.

745 Tolman HL (1997) User manual and system documentation of WAVEWATCH-III version 1.15. NOAA /
746 NWS / NCEP / OMB Technical Note 151, 97 pp.

747 Tolman HL (1999) User manual and system documentation of WAVEWATCH-III version 1.18. NOAA
748 / NWS / NCEP / OMB Technical Note 166, 110 pp.

749 Tolman HL (2009) User manual and system documentation of WAVEWATCH III version 3.14. NOAA /
750 NWS / NCEP / MMAB Technical Note 276, 194 pp.

751 Tolman HL, Chalikov, DV (1996) Source terms in a 3rd generation wind-wave model. *J. Phys.*
752 *Oceanogr.*, 26:2497-2518.

753 Wilby R L, Troni J, Biot Y, Tedd L, Hewitson BC, Smith DM, Sutton RT (2009), A review of climate risk
754 information for adaptation and development planning, *International Journal of Climatology*,
755 29(9):1193-1215.

756 Whetton P, Hennessy K, Clarke J, McInnes K, Kent K (2012) Use of Representative Climate Futures
757 in impact and adaptation assessment, *Climatic Change*, 115(3-4):433-442.

758 Wong PP (1992) Impact of a sea level rise on the coasts of Singapore: preliminary observations
759 *Journal of Southeast Asian Earth Sciences*, Vol. 7, No. 1, pp. 65-70, 1992.

760

761

762

763

764

765

766

767

768

769

770

771

772

773

774

775

776

777

778

779

780

781 **Tables**

782 **Table 1:** Summary table of methodologies employed to estimate the different components of sea level
 783 rise at Singapore, including scaling factors used to convert global mean trends into local trends.

Component	Methodology
1. Oceanographic sea level	CMIP5 climate model estimates of global thermal expansion and dynamic sea level are combined for each model. Differences between the two periods 1986-2005 and 2081-2100 are computed for each climate change scenario. A multi-model mean and spread in this component is extracted for Singapore using a nearest-neighbour approach. Time series are constructed based on the assumption that the change signal emerges proportionally to AR5 estimates of global thermal expansion.
2. Glaciers	Time series of global sea level rise from AR5 data files are scaled by a factor of 1.11, according to the spatial fingerprint information provided by Slangen et al. (2014).
3. Greenland surface mass balance	Time series of global sea level rise from AR5 data files are scaled by a factor of 1.14, according to the spatial fingerprint information provided by Slangen et al. (2014).
4. Antarctica surface mass balance	Time series of global sea level rise from AR5 data files are scaled by a factor of 1.13, according to the spatial fingerprint information provided by Slangen et al. (2014).
5. Greenland dynamics	Time series of global sea level rise from AR5 data files are scaled by a factor of 1.16, according to the spatial fingerprint information provided by Slangen et al. (2014).
6. Antarctica dynamics	Time series of global sea level rise from AR5 data files are scaled by a factor of 1.19, according to the spatial fingerprint information provided by Slangen et al. (2014).
7. Land water storage	Time series of global sea level rise from AR5 data files are scaled by a factor of 0.81, according to the spatial fingerprint information provided by Slangen et al. (2014).
8. Glacial isostatic adjustment (GIA)	Estimate based on ICE5G (Peltier, 2004) model as provided by Slangen et al. (2014).
9. Inverse barometer	Assessed from AR5 supplementary data files. Not included in projections, given the negligible contribution.

784

785

786

787

788

789

790

791 **Table 2:** Median values and *likely* (in IPCC calibrated language – see section 2.1) ranges (square
792 brackets) for projections of time mean sea level rise and its contribution in metres for 2081-2100
793 relative to 1986-2005 for Singapore and the global average (as reported in Table 13.5 of AR5, Church
794 et al., 2013).
795

Sea level component	RCP4.5 change (m)		RCP8.5 change (m)	
	Singapore	Global	Singapore	Global
Expansion / Oceanographic	0.20 [0.12,0.27]	0.19 [0.14,0.23]	0.27 [0.18,0.36]	0.27 [0.21,0.33]
Glaciers	0.14 [0.07,0.22]	0.12 [0.06,0.19]	0.18 [0.10,0.26]	0.16 [0.09,0.23]
Greenland Surface Mass Balance	0.05 [0.01,0.18]	0.04 [0.01,0.09]	0.08 [0.03,0.18]	0.07 [0.03,0.16]
Antarctica Surface Mass Balance	-0.02 [-0.06,-0.01]	-0.02 [-0.05,-0.01]	-0.05 [-0.08,-0.01]	-0.04 [-0.07,-0.01]
Greenland Dynamics	0.05 [0.01,0.07]	0.04 [0.01,0.06]	0.06 [0.02,0.08]	0.05 [0.02,0.07]
Antarctica Dynamics	0.08 [-0.01,0.19]	0.07 [-0.01,0.16]	0.08 [-0.01,0.19]	0.07 [-0.01,0.16]
Land Water	0.03 [-0.01,0.07]	0.04 [-0.01,0.09]	0.03 [-0.01,0.07]	0.04 [-0.01,0.09]
GIA	-0.03	N/A	-0.03	N/A

796

797

798 **Table 3:** Estimates of global sea level rise from the IPCC AR5 (Church et al., 2013) alongside our
799 regional estimates for Singapore. Following the definitions in AR5, there is a 66-100% chance that
800 future sea level rise will fall within the ranges quoted. Based on current understanding, only the
801 collapse of marine-based sectors of the Antarctic ice sheet, if initiated, could cause global mean sea
802 level to rise substantially above the *likely* range during the 21st century. This potential additional
803 contribution cannot be precisely quantified but there is medium confidence that it would not exceed
804 several tenths of a meter of sea level rise during the 21st century (Church et al, 2013).

805

Scenario		2050			2100		
		Central	Lower	Upper	Central	Lower	Upper
RCP4.5	Global	0.23	0.17	0.29	0.53	0.36	0.71
	Singapore	0.22	0.14	0.29	0.52	0.29	0.73
RCP8.5	Global	0.25	0.19	0.32	0.74	0.52	0.98
	Singapore	0.25	0.17	0.32	0.74	0.45	1.02

806

807

808

809

810

811

812 **Table 4:** Projected century-scale trends in skew surge for five return periods (excluding
813 mean sea level change). Units are mm per century.

Period/years	2	20	100	1000	10000
Lower	-20	-40	-63	-90	-120
Central	0	-10	-20	-20	-30
Upper	20	20	30	50	60

814

815

816 **Table 5:** Projected century-scale trends in significant wave height for five return periods due to
817 storminess changes (mm per century, to two decimal places).

Period/years	2	20	100	1000	10000
Lower	-15	-460	-730	-1260	-2030
Central	-30	-140	-220	-390	-620
Upper	80	190	290	490	780

818

819

820

821

822

823

824

825

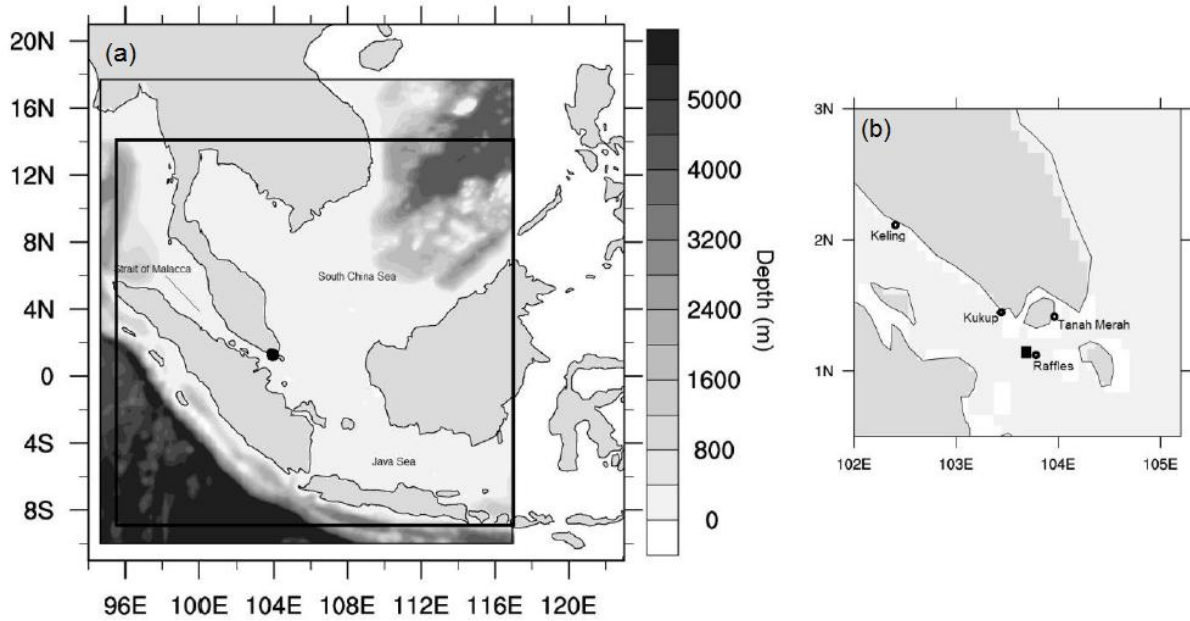
826

827

828

829 **Figures**

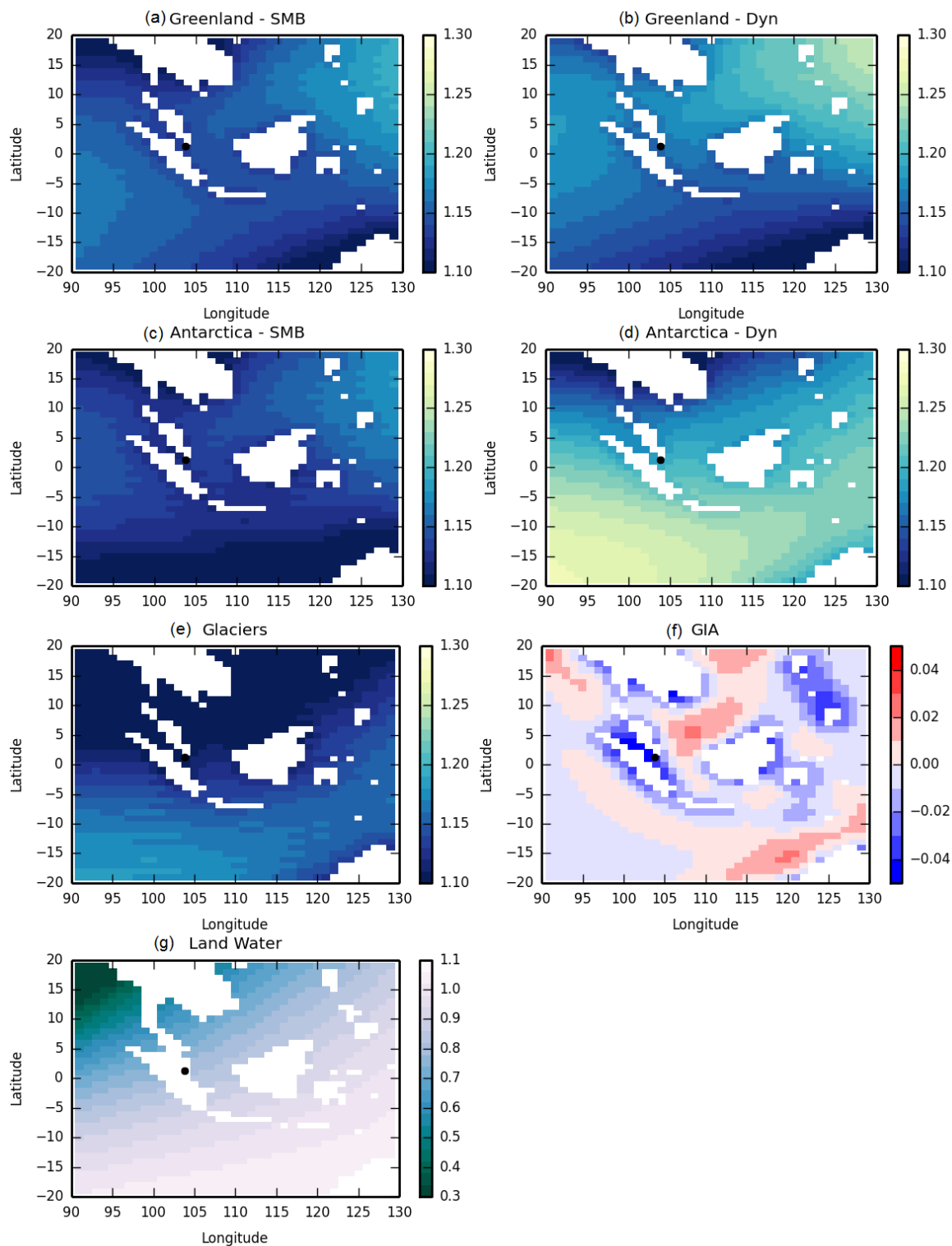
830



831

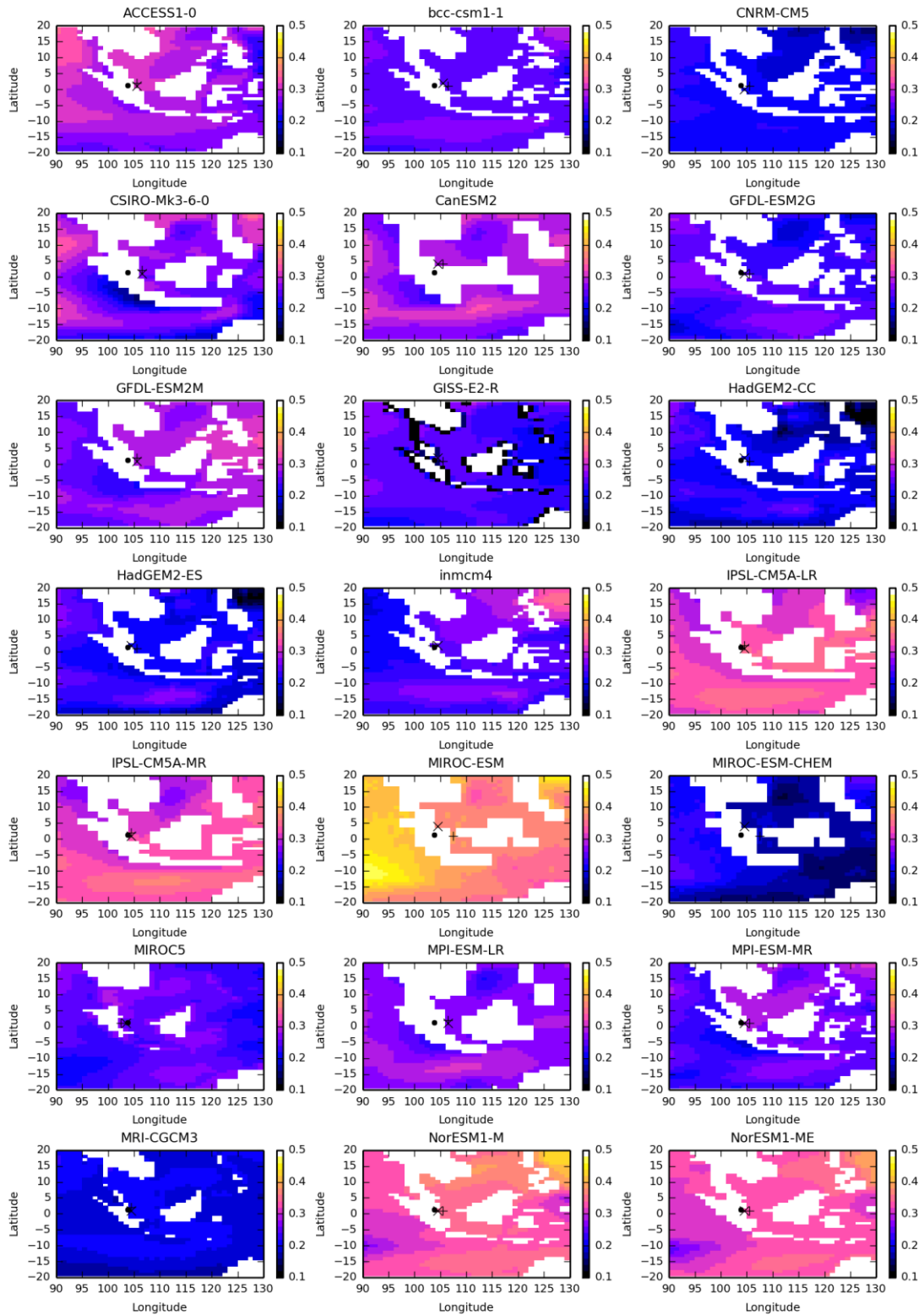
832 **Figure 1:** (a) Bathymetric map showing the location of Singapore (black circle) in relation to
833 the climate model domain (outermost square), the surge model domain (shaded depth
834 contours), and the wave model domain (innermost square). (b) Map of Singapore showing
835 the location of tide gauge meters utilised for model validation, and showing the location of
836 grid point 'a' as referred to in the results section (black rectangle).

837



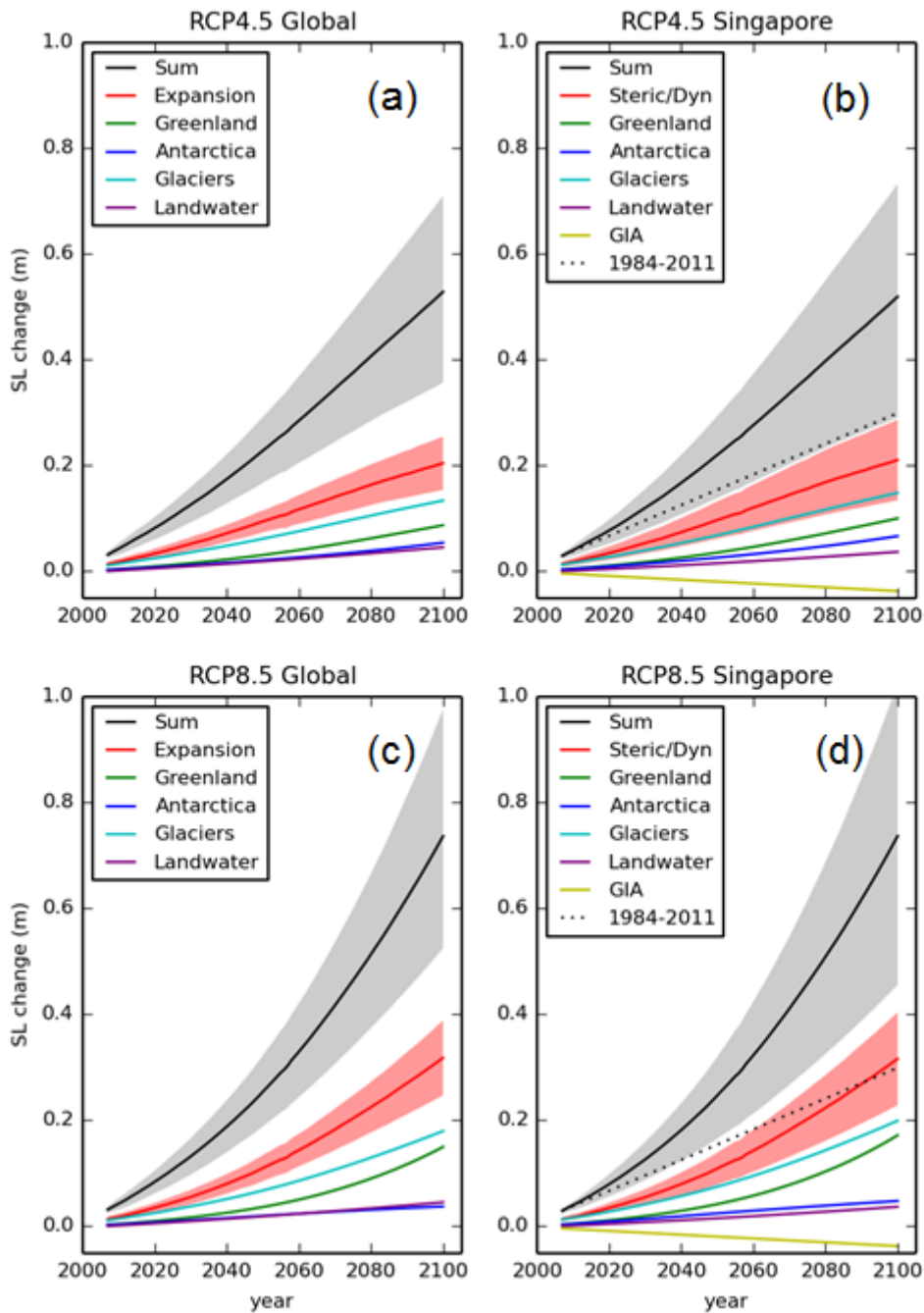
838

839 **Figure 2:** Spatial fingerprints for changes in (a) Greenland surface mass balance, (b)
 840 Greenland dynamical change, (c) Antarctica surface mass balance, (d) Antarctica dynamical
 841 change, (e) glaciers, (f) glacial isostatic adjustment and (g) changes in land water use. Panels
 842 a-e represent the ratio of local relative sea level change per unit of GMSL rise associated
 843 with mass input to the oceans. The location of Singapore is shown by the black circle.
 844 Source: Slangen *et al.* (2014).



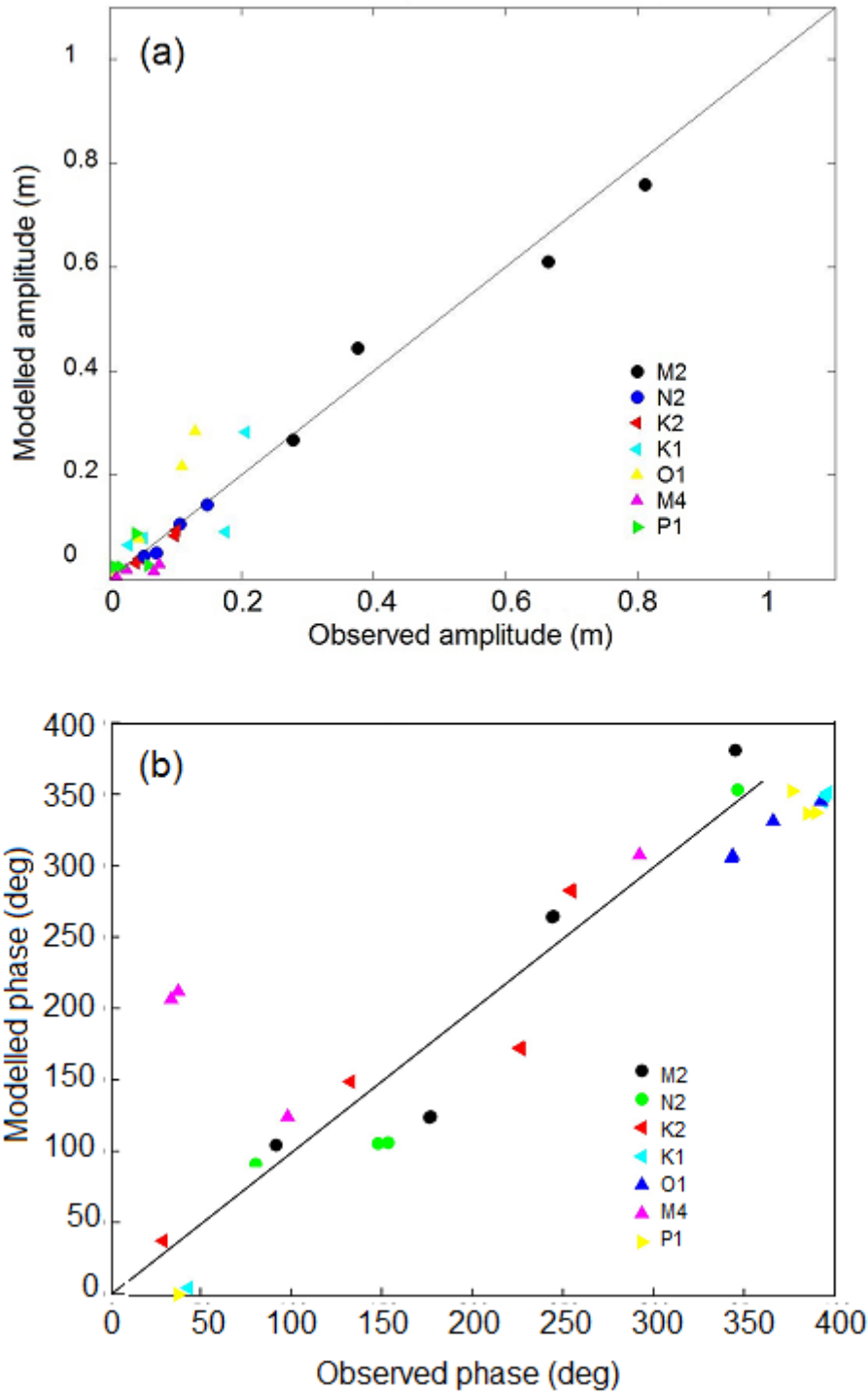
845

846 **Figure 3:** Projections of steric/dynamic sea level rise (metres) for 21 CMIP5 models under
 847 RCP8.5, computed as the difference between 1986-2005 and 2081-2100. The location of
 848 Singapore is shown by the black circle. The primary and secondary grid boxes used to extract
 849 time mean sea level for Singapore are shown by an × and +, respectively. Note the grid box
 850 selections for GISS-E2-R are away from potential problem areas for the land mask.



852

853 **Figure 4:** Projections of sea level rise relative to 1986-2005 and its contributions as a
 854 function of time for (a) global mean sea level (RCP4.5), (b) Singapore region (RCP4.5), (c)
 855 global mean sea level (RCP8.5) and (d) Singapore region (RCP8.5). Lines show the median
 856 projections. The likely ranges for the total and thermal expansion or steric/dynamic sea level
 857 changes are shown by the shaded regions. The contributions from ice sheets include the
 858 contributions from ice sheet rapid dynamical change. The dotted line shows an
 859 extrapolation of the observed 1984-2011 rate of sea level change for the Singapore Strait
 860 reported by Tkalich et al. (2013).



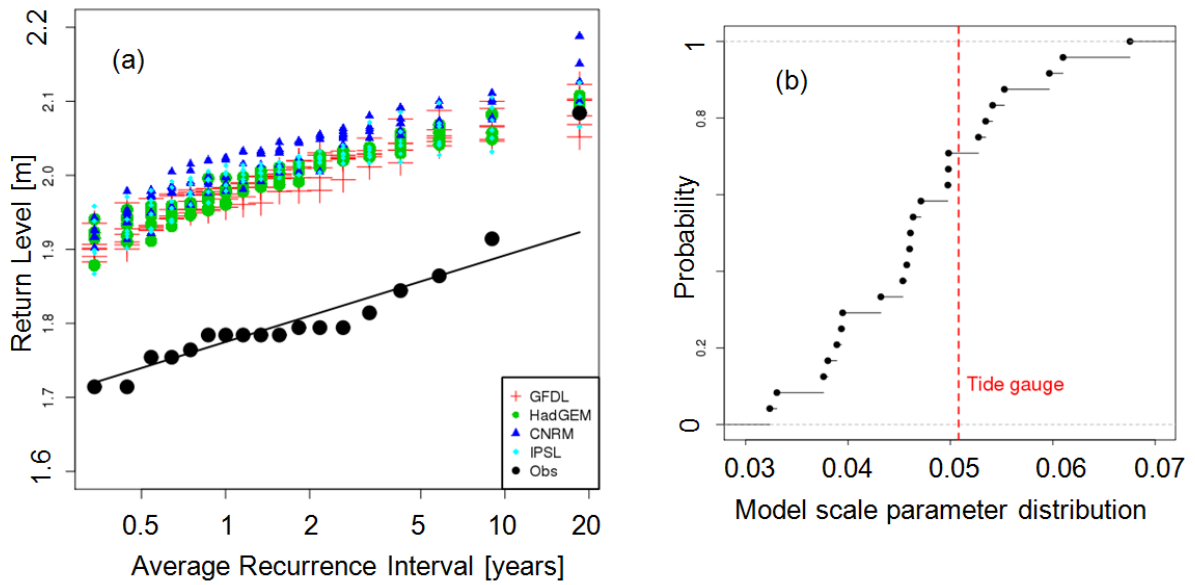
861

862

863 **Figure 5:** Comparison of modelled and observed (a) tidal amplitude and (b) tidal phase at 4
 864 tide gauge stations close to Singapore (Keling, Tanah Merah, Raffles lighthouse and Kukup)
 865 station locations are marked in Figure 1.

866

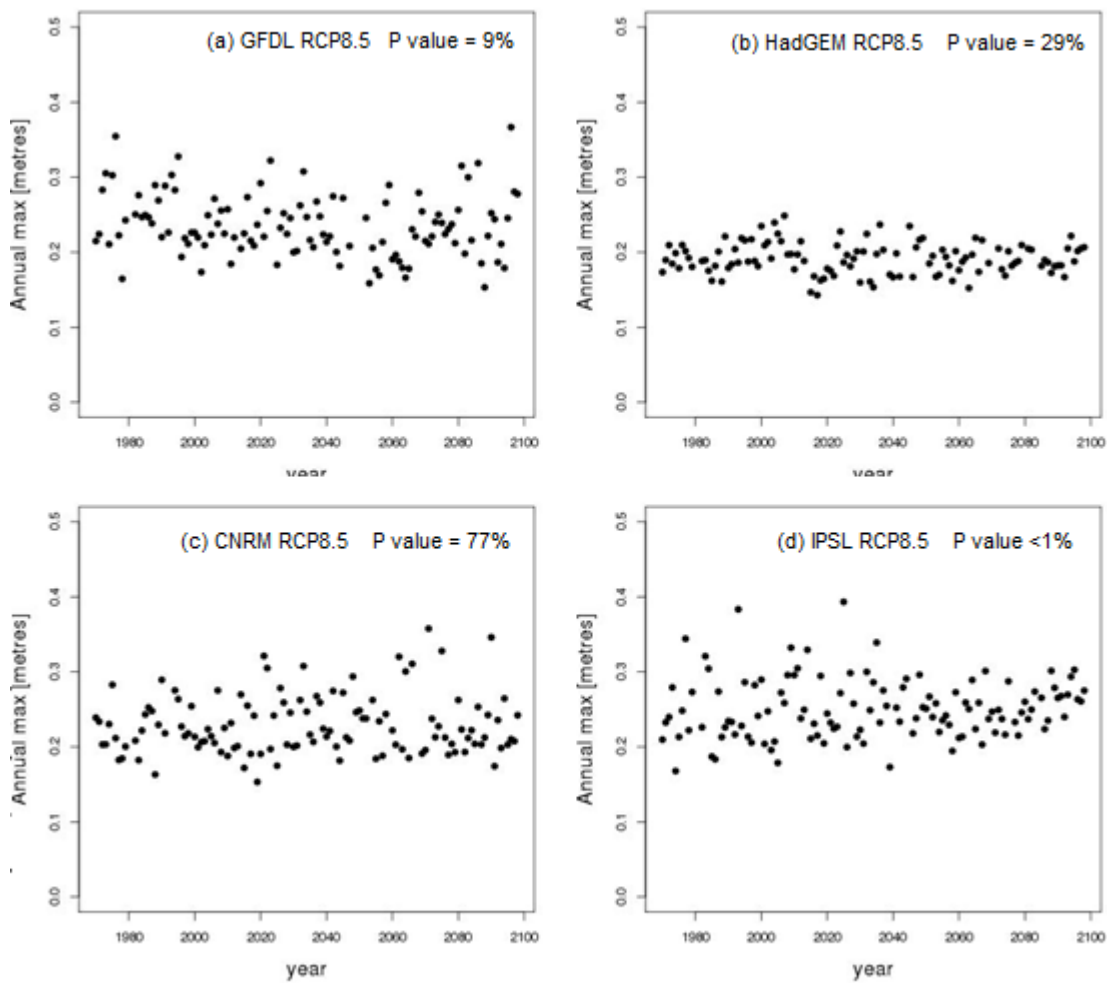
867



868

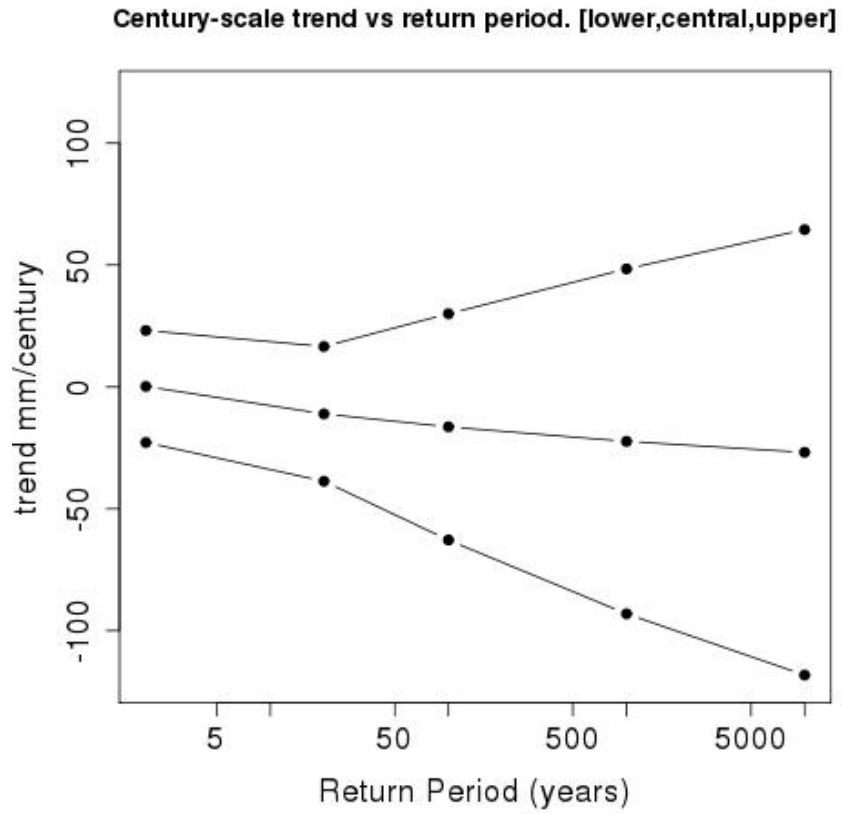
869 **Figure 6:** (a) Empirical return level data of extreme water level based on 18 years of tide
870 gauge data from Raffles Light House (1996-2013), and 18-year long samples from the model
871 simulations at grid point 'a'. The fitted Gumbel distribution of the observations is shown by
872 the straight line. (b) Empirical cumulative density function of the scale parameters of the
873 model samples, showing that the scale parameter of the tide gauge data sits well within the
874 model distribution.

875



876

877 **Figure 7:** Annual maxima skew surge obtained from the (a) GFDL, (b) HadGEM, (c) CNRM,
 878 and (d) IPSL forced simulations. The P value indicates the statistical significance of the
 879 improvement in fit when using a non-stationary GEV model: a large P value indicates little
 880 improvement; a small P value indicates significant improvement.



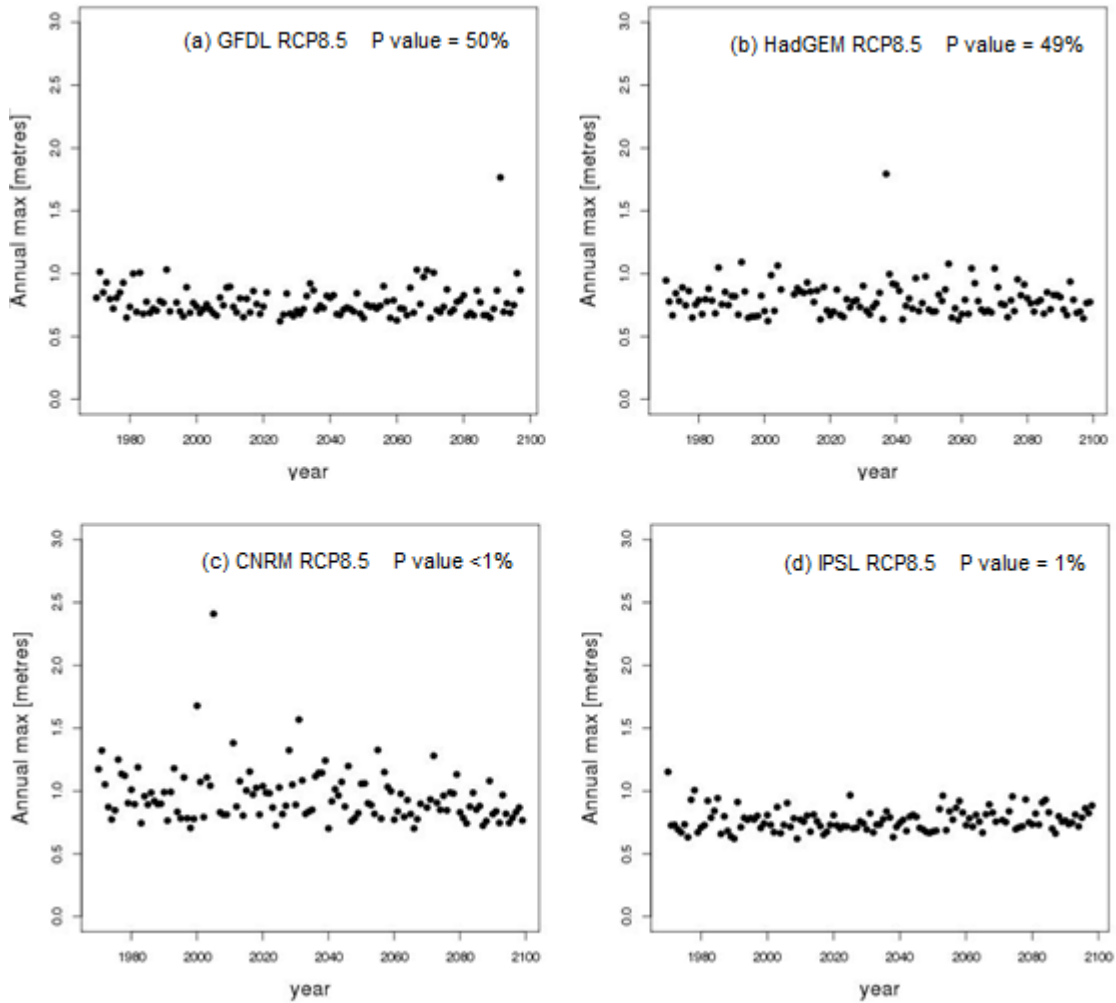
881

882

883 **Figure 8:** Projected century-scale trends in skew surge for five return periods due to
 884 storminess changes only (i.e. excluding mean sea level change) (mm per century). Central,
 885 lower and upper estimates are shown.

886

887

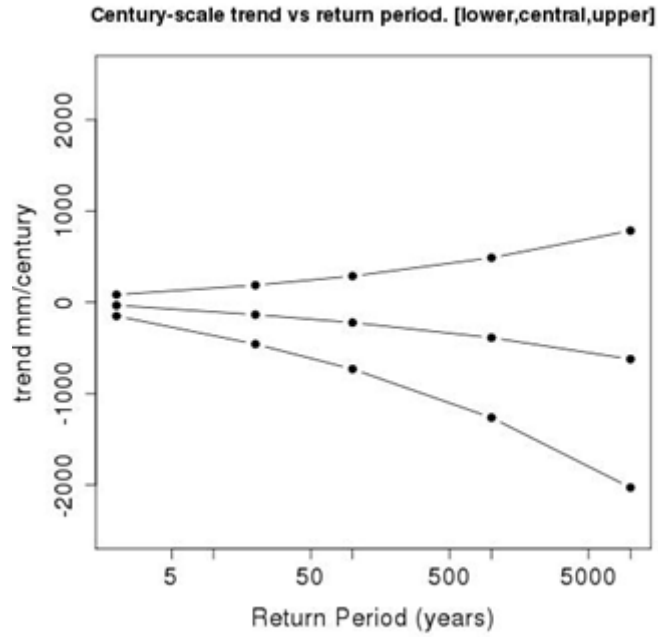


888

889 **Figure 9:** Simulated annual maxima of significant wave height (metres) obtained from the (a)
 890 GFDL, (b) HadGEM, (c) CNRM, and (d) IPSL forced simulations. The P value indicates the
 891 statistical significance of the improvement in fit when using a non-stationary GEV model: a
 892 large P value indicates little improvement; a small P value indicates significant improvement.

893

894

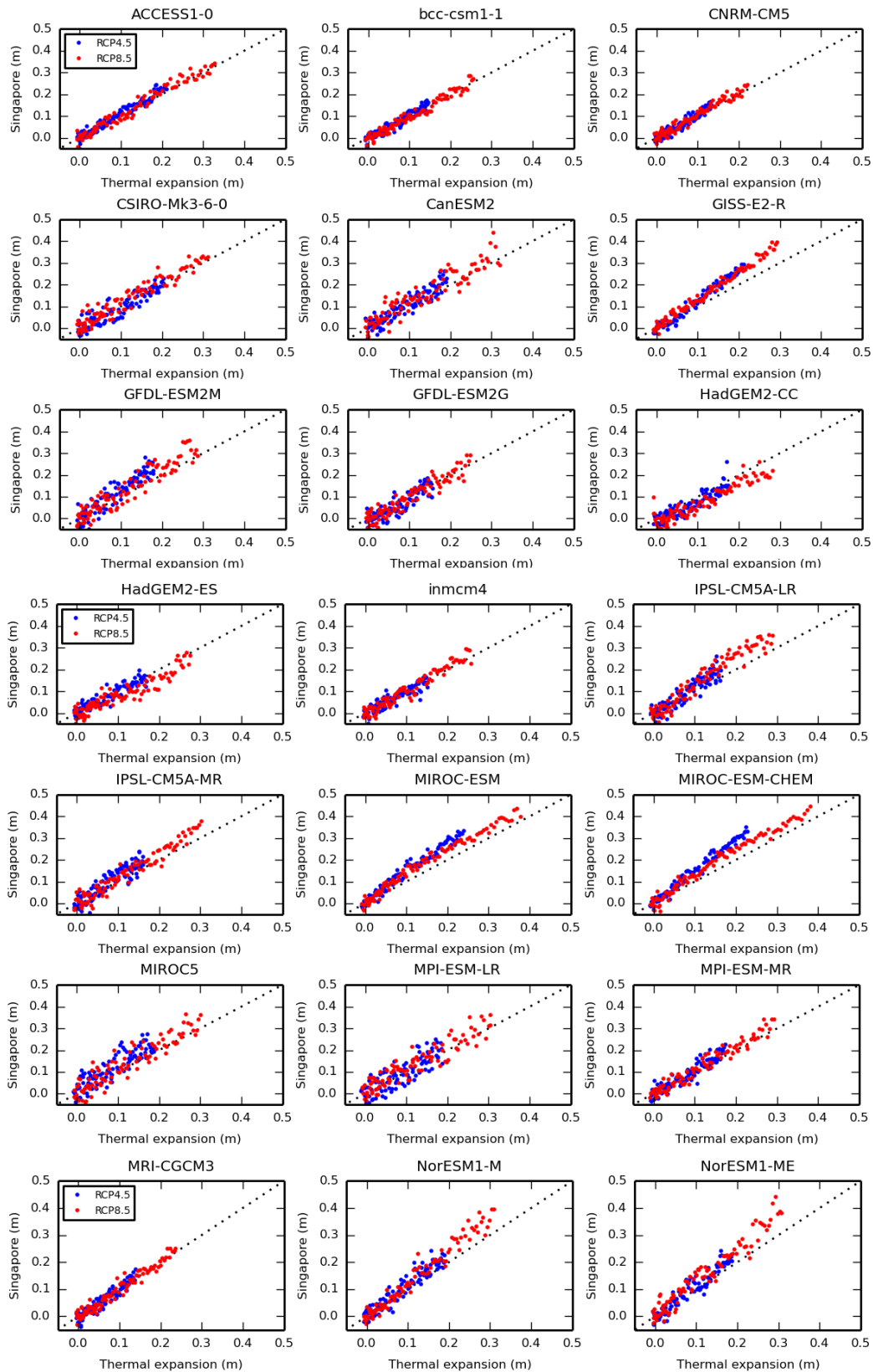


895

896 **Figure 10:** Projected century-scale trends in significant wave height for five return periods
 897 due to storminess changes only (i.e. excluding mean sea level change) (mm per century).
 898 Central, lower and upper estimates are shown.

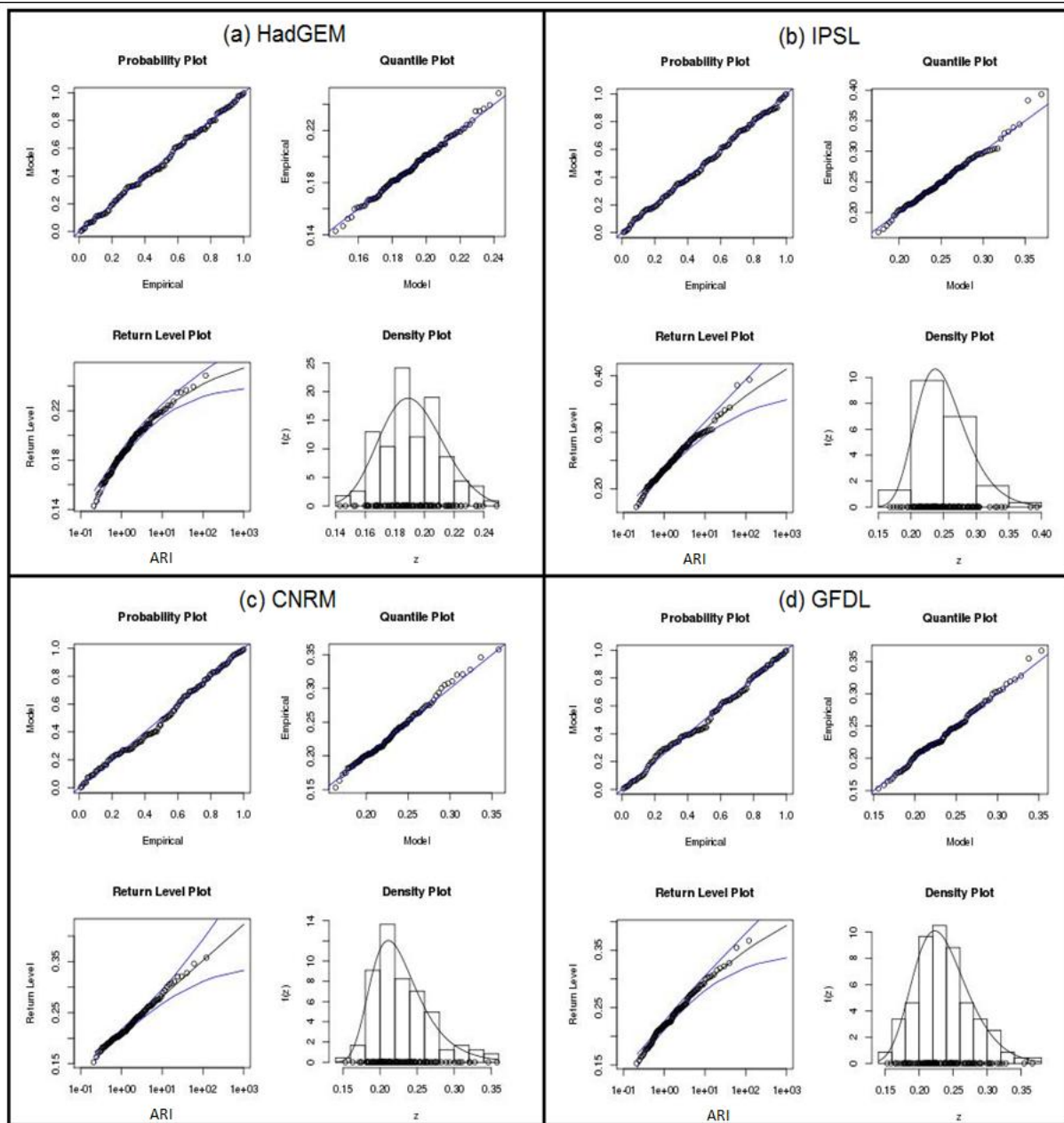
899 **Appendix**

900



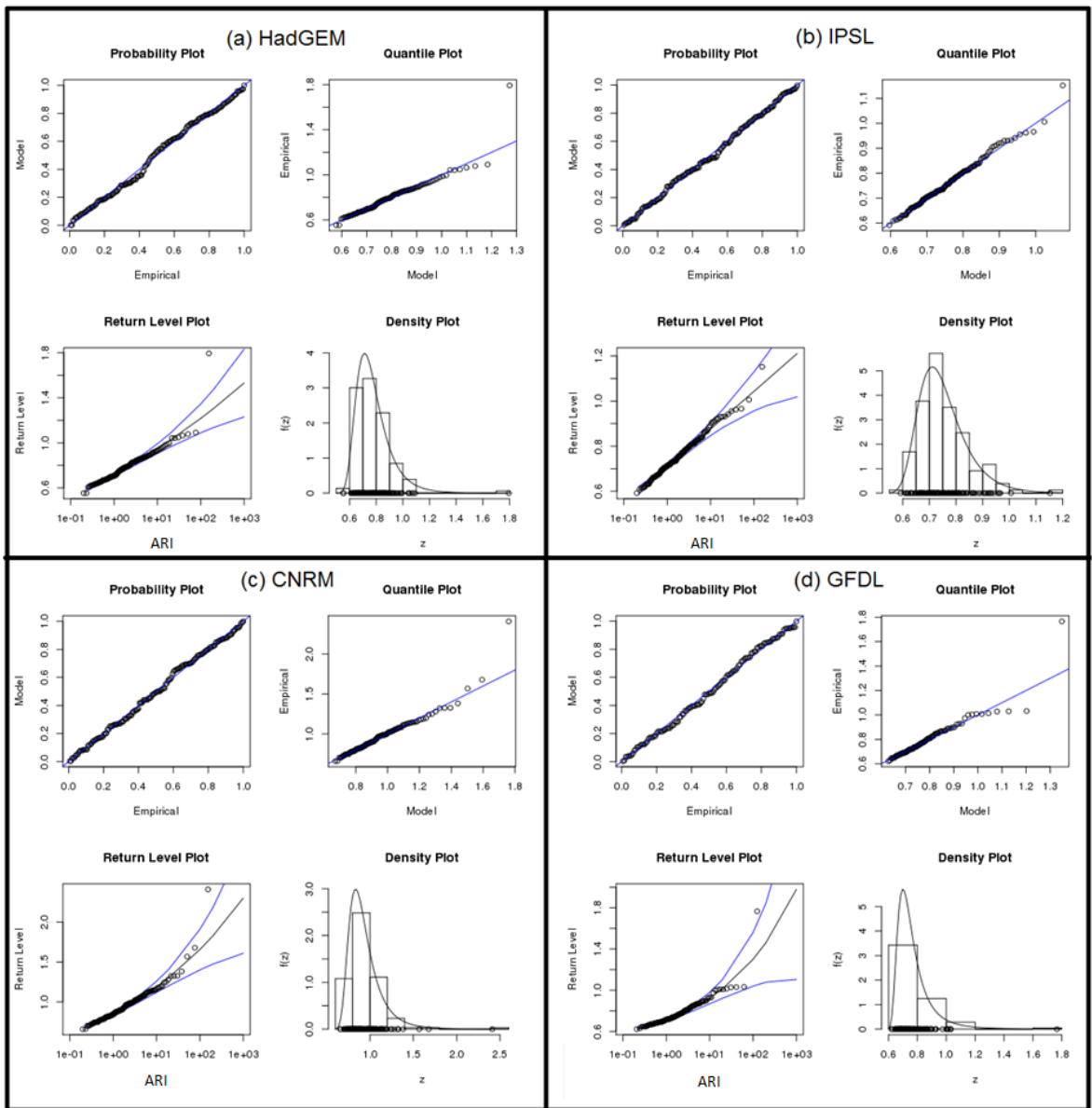
901

902 **Figure A1:** Regression between local oceanographic sea level change (due to steric plus dynamic
 903 processes) and global thermal expansion terms for each CMIP5 model under RCP 4.5 and RCP 8.5.



905

906 **Figure A2:** Standard diagnostic plots for stationary fit to skew surge annual maxima from (a)
 907 HadGEM2-ES, (b) IPSL, (c) CNRM, and (d) GFDL simulations. The quantile and probability plots
 908 compare the theoretical distribution fitted to the data with the actual data and give an indication of
 909 confidence in the fit of the return period.



910

911 **Figure A3:** Standard diagnostic plots for stationary fit to significant wave height annual
 912 maxima from (a) HadGEM2-ES, (b) IPSL, (c) CNRM and (d) GFDL simulations. The quantile and
 913 probability plots compare the theoretical distribution fitted to the data with the actual data and give an
 914 indication of confidence in the fit of the return period.

915